Journal of Controlled Release 352 (2022) 776–792

Contents lists available at ScienceDirect

Journal of Controlled Release

journal homepage: www.elsevier.com/locate/jconrel

Perimeter and carvacrol-loading regulate angiogenesis and biofilm growth in 3D printed PLA scaffolds

Xián Farto-Vaamonde [a], Luis Diaz-Gomez [a], Ana Parga [b], Ana Otero [b], Angel Concheiro [a], Carmen Alvarez-Lorenzo [a,*]

[a] Departamento de Farmacología, Farmacia y Tecnología Farmacéutica, I+D Farma Group (GI-1645), Facultad de Farmacia, Instituto de Materiales (iMATUS), and Health Research Institute of Santiago de Compostela (IDIS), Universidade de Santiago de Compostela, 15782 Santiago de Compostela, Spain
[b] Departamento de Microbiología y Parasitología, Facultad de Biología, Edificio CiBUS, Universidade de Santiago de Compostela, 15782 Santiago de Compostela, Spain

ARTICLE INFO

Keywords:
3D printing
Polylactic acid (PLA)
Carvacrol
Anti-biofilm
In ovo
Micro-CT
Isothermal calorimetry

ABSTRACT

Carvacrol is a natural low-cost compound derived from oregano which presents anti-bacterial properties against both Gram-positive and Gram-negative bacteria. In this work, carvacrol-loaded PLA scaffolds were fabricated by 3D printing as platforms to support bone tissue regeneration while preventing biofilm development. Scaffolds were printed with or without a perimeter (lateral wall) mimicking the cortical structure of bone tissue to further evaluate if the lateral interconnectivity could affect the biological or antimicrobial properties of the scaffolds. Carvacrol incorporation was performed by loading either the PLA filament prior to 3D printing or the already printed PLA scaffold. The loading method determined carvacrol localization in the scaffolds and its release profile. Biphasic profiles were recorded in all cases, but scaffolds loaded post-printed released carvacrol much faster, with 50–80% released in the first day, compared to those containing carvacrol in PLA filament before printing which sustained the release for several weeks. The presence or absence of the perimeter did not affect the release rate, but total amount released. Tissue integration and vascularization of carvacrol-loaded scaffolds were evaluated in a chorioallantoic membrane model (CAM) using a novel quantitative micro-computed tomography (micro-CT) analysis approach. The obtained results confirmed the CAM tissue ingrowth and new vessel formation within the porous structure of the scaffolds after 7 days of incubation, without leading to hemorrhagic or cytotoxic effects. The absence of lateral wall facilitated lateral integration of the scaffolds in the host tissue, although increased the anisotropy of the mechanical properties. Scaffolds loaded with carvacrol post-printing showed antibiofilm activity against *Staphylococcus aureus* and *Pseudomonas aeruginosa* as observed in a decrease in CFU counting after biofilm detachment, changes in metabolic heat measured by calorimetry, and increased contact killing efficiency. In summary, this work demonstrated the feasibility of tuning carvacrol release rate and the amount released from PLA scaffolds to achieve antibiofilm protection without altering angiogenesis, which was mostly dependent on the perimeter density of the scaffolds.

1. Introduction

Bone diseases (e.g., arthritis, osteoporosis, bone tumors) affect millions of people worldwide, and this number is expected to increase in the next few years due to ageing population [1,2]. Autograft and allograft shortage has motivated intense research on the biofabrication of three-dimensional (3D) biodegradable scaffolds for bone regeneration. 3D printing technologies, particularly Fused Filament Fabrication (FFF), offer relevant advantages compared to conventional procedures to prepare bone scaffolds. Biodegradable thermoplastic polymers are affordable and highly available and avoid the need for a second surgery to remove the implant from the patient body, evading the associated risks. Furthermore, since 3D printing is an additive manufacture procedure there is no waste of material and the scaffold can be personalized to each patient to fit into the injury shape, the number and interconnection of pores can be finely tuned to favor cell migration (between 100 and 500 μm), and the mechanical resistance can be matched to the target tissue [3–5].

Preclinical assessment of the vascularization and integration of biodegradable scaffolds is key to predict and understand the outcome of

* Corresponding author.
E-mail address: carmen.alvarez.lorenzo@usc.es (C. Alvarez-Lorenzo).

https://doi.org/10.1016/j.jconrel.2022.10.060
Received 13 July 2022; Received in revised form 7 October 2022; Accepted 30 October 2022
Available online 11 November 2022

novel biomaterials scaffolds before their clinical application. Recently, chick chorioallantoic membrane (CAM) models have been introduced in the evaluation of implantable materials as an effort to replacing, reducing, and refining the use of animals in preclinical studies (3Rs principle) [6]. Indeed, the CAM represents a relevant preclinical model to evaluate the angiogenic and biological behavior of biomaterials in regenerative medicine [7]. However, so far most studies failed to address the quantitative examination of tissue development and vessel formation in 3D scaffolds. The frequently used histological approaches to quantify CAM-scaffold integration and vascularization lack of spatial resolution and provide an incomplete picture of the regenerative environment. As an alternative, micro-computed tomography (micro-CT) may offer advanced possibilities as a non-destructive, high-resolution tool to evaluate the extent of tissue integration and angiogenesis within porous scaffolds [8].

Another of the main challenges related to the success of scaffold-based therapies is to avoid bacteria colonization of the surface. Scaffold-related infections occur in approximately 2–5% of orthopaedic implantation procedures, and up to 30% in the case of open bone fractures [9]. Bacteria have been shown to easily attach and colonize scaffolds surface, secreting a polysaccharide matrix to form a biofilm. Biofilm formation allows microorganisms to organize themselves into a three dimensional, structured, interconnected, and communicated community that exhibits increased resistance to antibiotics and the host immune system [10,11]. This resistance leads to chronic inflammation and infection in the surrounding tissue, hindering tissue regeneration, and compromising patient's life. Bone-related infections cause scaffold failure and/or longer recovery and hospitalization times, as well as increased medical costs. While self-limited inflammatory process associated to injuries (e.g., bone fracture or bone surgery) promotes angiogenesis and cell recruitment [12], bacterial-derived chronic inflammation may delay the regeneration process and even extend the injured area [13]. In the process of biofilm formation, bacterial adhesion to the medical device is a key first step, with many factors playing a role, including bacterial species and strain, morphology, topography, and physicochemical properties of the biomaterial, and trace chemical residues or glycoproteins (i.e., fibronectin) from the patient fluids. Gram-positive bacteria account for most orthopaedic related infections, with *Staphylococcus aureus* and *Staphylococcus epidermidis* being responsible for more than half of the cases [14]. While Gram-negative bacteria infections are less frequent, their pathologies are more severe and difficult to treat, especially for *Pseudomonas aeruginosa* [15]. Both *S. aureus* and *P. aeruginosa* are classified as priority pathogens by the World Health Organization for the development of novel antibiotics due to the increasing appearance of pan-resistant strains [16].

In addition to mechanical support, scaffolds can also serve as platforms for local antimicrobial delivery [17]. Nonetheless, drawbacks associated to the incorporation of single antibiotic drugs with narrow activity spectrum and the failure to achieve minimum inhibitory concentrations can contribute to increasing bacteria resistance [18]. Furthermore, the potential toxicity of antibiotics to developing tissue and in particular osteoblasts needs to be considered [19]. The search for novel antimicrobials and synergic approaches is gaining importance in the treatment and prevention of bacterial infections [20,21]. Essential oils are pointed out as successful alternatives against bacterial biofilm formation, alone or as adjuvants together with antibiotics [22,23]. Carvacrol (2-methyl-5-(1-methylethyl)phenol) is a natural monoterpenoid phenol found in the essential oil of oregano species, among other plants, and displays a wide antimicrobial and antibiofilm spectrum against bacteria, yeast and fungi [24,25]. Carvacrol is a Generally Recognized As Safe (GRAS) substance by the Food and Drugs Administration (FDA) and the Council of Europe, and frequently used a flavouring, aromatic and preservative agent in the food industry [24,26]. Nonetheless, little research in the incorporation of carvacrol in implantable fibers [27,28] and films and resins for food industry has been done [29–31] and its use has not been considered yet in 3D printed scaffolds for tissue regeneration. In addition to the antimicrobial activity, carvacrol has been found able to modulate the inflammatory phase of wound healing and to promote angiogenesis and host cell growth [32].

Since scaffold colonization has been described as a competition (or race) between host cells and bacteria [33], the present work relied on the hypothesis of that hindering bacteria adhesion by means of carvacrol release while at the same time promoting the colonization by host cells by tuning the physical structure of the scaffold perimeter may provide synergic outcomes in terms of both biofilm prevention and neotissue formation. The faster and more efficient integration of host cells may act itself as a barrier against bacteria colonization [34]. Thus, the aim of this work was to investigate whether the incorporation of carvacrol to 3D printed PLA scaffolds can endorse the scaffolds with antibacterial and antibiofilm properties without compromising their structural and biological performance. Scaffolds with and without a perimeter (i.e., a wall of material laterally surrounding the scaffold) were printed. The presence or absence of perimeter could determine the lateral open porosity and the mechanical properties of the scaffolds, which in turn may affect carvacrol release rate and scaffold integration in living tissues. It has been previously shown that the strategy used to incorporate hydrophilic crystalline drugs in a 3D printed scaffold may notably determine its release pattern [35]. Differently, there is a lack of information on the incorporation of essential oils, which are very hydrophobic and volatile, on polymeric filaments. In this work, carvacrol was incorporated in PLA scaffolds using two different approaches to evaluate their effect on carvacrol release, antibiofilm properties and angiogenesis: (i) drug loading in PLA filaments prior to 3D printing, or (ii) a post-printing loading consisting in the incorporation of carvacrol in 3D printed PLA scaffolds. The obtained scaffolds were characterized in vitro for their porous structure and mechanical properties, release kinetics, and cytotoxicity. A CAM assay model was used to provide a more in-depth assessment of the biological performance of the scaffolds in an in vivo environment. The assessment of the cell infiltration and vascularization was carried out using a novel non-destructive micro-CT approach based on the volumetric quantification of CAM tissue and vessel architecture developed within the scaffolds. The antimicrobial properties of the scaffolds against *S. aureus* and *P. aeruginosa* were evaluated both by CFU counting and by real-time monitoring of metabolic heat using isothermal microcalorimetry. Calorimetric techniques, although still incipiently applied in the field of the regenerative medicine, may provide more precise, direct and robust information on the performance of the scaffolds minimizing risks of bias associated to subsequent handling and steps of traditional microbiological techniques [36,37].

2. Materials and methods

2.1. Materials

Polylactic acid (PLA) filament (diameter 1.75 mm) was purchased from Createc3D (Granada, Spain; Mw 181,623 Da (PDI 1.14) [35]). Carvacrol was from Sigma Aldrich (St. Louis MO, USA). Methanol and Luria-Bertani Broth (Miller) (LB) were from Scharlab (Barcelona, Spain), ethyl acetate from Merck (Darmstadt, Germany) and ethanol from VWR Chemicals (Radnor, PA, USA). Ultrapure water (resistivity >18.2 MΩ cm) was obtained by reverse osmosis (MilliQ®, Millipore Ibérica, Madrid, Millipore Spain). Dulbecco's Modified Eagle Medium (DMEM), fetal bovine serum (FBS) and Anti-Anti (antibiotic-antimycotic) were from Gibco (Thermofisher, Waltham, MA, USA). Cell Counting Kit-8 (CCK-8) was from Dojindo (Kumamoto, Japan). 3-(4,5-dimethylthiazol-2-yl)-2,5-diphenyltetrazolium bromide (MTT) was from Merck KGaA (Darmstadt, Germany). Live/Dead® BacLight™ viability assay was from ThermoFisher. Tryptic Soy Broth (TSB-1) was from Oxoid (Hampshire, UK). Sylgard 184 (silicone rubber) was from Dow Chemicals (Michigan, USA). All other chemicals and reagents were from Sigma Aldrich (St. Louis, MO, USA) and used as supplied.

2.2. Scaffold printing

PLA porous scaffolds were prepared using a BioV1 3D printer (Regemat3D, Granada, Spain). A cylindrical template of 10 mm diameter, 5 mm height, 0.6 mm pore size and 0.35 mm layer height, with a woodpile internal pattern was designed with Regemat Designer Software and used to print the scaffolds. The extrusion temperature was set at 220°C with a printing flow speed of 1.20 mm/s. The printer was used in its standard configuration, equipped with a 0.40 mm nozzle. A second set of scaffolds was also printed as previously described but disregarding the external contour, i.e., without the lateral wall perimeter (scaffold without perimeter). A scheme of the fiber layout is provided in Fig. S1 (Supplementary Information).

2.3. Carvacrol loading

Carvacrol loading was performed by soaking either raw PLA filaments (length ~ 12 cm) or 3D printed blank scaffolds in a 5% or 10% *v*/v carvacrol solution in methanol:ethyl acetate 50:50 v/v mixture, at 37°C, protected from light and under oscillatory movement (shaker at 170 rpm) for 72 h. PLA filaments (3 pieces per vial) were placed in test tubes with screw cap containing 28 mL of carvacrol solution completely covering the filament surface. After incubation, filaments were dried in oven at 50°C for 24 h and then fed into the 3D printer to produce carvacrol-loaded scaffolds. Separately, blank scaffolds were placed individually in vials with 5 mL of a carvacrol solution as described above. After incubation, carvacrol-loaded PLA filaments and scaffolds were dried in oven at 50°C for 24 h.

The total amount of carvacrol loaded in the scaffolds was quantified as follows. Scaffolds ($n = 3$) were immersed in 5 mL of methanol:ethyl acetate (50:50 *v*/v) mixture and kept at 37°C for 10 days, under oscillatory movement (180 rpm) and protected from light. At predetermined times, aliquots of 0.1 mL were withdrawn from medium and diluted 1:20 with ethanol:water (50:50 *v*/v) mixture. Absorbance was measured at 273 nm (Agilent 8453 UV/Vis spectrophotometer, Waldbronn, Germany). The withdrawn volume was replaced with fresh medium.

2.4. Carvacrol release

Scaffolds (three replicates of each condition) were individually placed in vials with 5 mL of ethanol:water (50:50 *v*/v) medium and then kept in a minishaker at 37°C under constant orbital movement (200 rpm) and protected from light. At predetermined times, 0.1 mL aliquots were withdrawn from medium and diluted accordingly before absorbance measurement at 273 nm (Agilent 8453 UV/Vis spectrophotometer). The withdrawn volume was replaced with fresh medium. The Korsmeyer-Peppas model [38] was used to fit carvacrol release profile in the log-log plot as follows:

$$Log\left(\frac{Mt}{M\infty}*100\right) = Log\ k + n\ Log\ t \quad (1)$$

In this equation, Mt/M_∞ represents the fraction of carvacrol released respect to the amount loaded, k is the release rate constant, and n is the diffusional exponent. The release profiles were analyzed considering two regions: region I comprised from time 0 to 8 h in case of PLA-CAR 10% scaffolds and to 24 h for F.PLA-CAR 10% and PLA-CAR 5% scaffold (<60% carvacrol released in all cases); while region II comprised the subsequent time values until 80% carvacrol released [27].

2.5. Structure analysis

Scaffold diameter and height were measured with a digital caliper (Fowler™, Newton, MA, USA). All scaffolds were measured, and results were expressed in terms of mean ± standard deviation of weight, height, and diameter. Morphological analysis of the scaffolds was conducted with an Olympus CKX53 microscope equipped with an Olympus EP50 digital camera (Shinjuku, Tokyo, Japan). Surface topography and 3D architecture of scaffolds were examined using field emission scanning electron microscopy (FESEM Ultra Plus, Zeiss, Oberkochen, Germany). Scaffolds were prepared for SEM by cryofracturing to obtain cross-section views. Scaffolds were placed on metal supports and sputter-coated with 10 nm thick iridium film (Q150T-S, Quorum Technologies, Lewes, UK) before visualization. The changes in the morphology of the fibers of the scaffolds was evaluated by SEM and optical microscopy after incubation for 18 months in PBS pH 7.4 at 37°C protected from light, following the procedures described before for the freshly printed scaffolds.

The structure of the scaffolds was analyzed by microcomputed tomography (micro-CT) using a Skyscan 1272 high resolution X-ray 3D micro-CT equipped with an 11 MP X-ray detector (Bruker, Kontich, Belgium). Scaffolds were imaged at 10 μm pixel resolution, 50 kV and 200 μA without filter. Projections were collected at 0.2° over 180° with an exposure time of 175 ms, and then reconstructed and analyzed using NRecon and CTAn software (Bruker, Kontich, Belgium), respectively. For 3D analysis, slices were converted into binary images using a threshold of 70–255 and a VOI of 60 mm^3 was chosen to evaluate total porosity, pore size and interconnectivity ($n = 5$).

Water contact angles were measured on 3D printed PLA sheets (10 × 10 mm squares without pores, 0.35 mm layer height, 4 layers). PLA sheets were loaded with carvacrol following the same procedure as for scaffolds. Treated PLA sheets (soaking in methanol:ethyl acetate 1:1 but without carvacrol) were also evaluated. A water drop (5 μL) was deposited on the material and one image per second was taken for 10 s with a Phoenix-300 plus video-based optical goniometer (SEO, Korea) ($n = 5$).

2.6. Crystallinity

X-ray powder diffraction (XRD) and differential scanning calorimetry (DSC) were used to identify and characterize the crystal structure and thermal stability of carvacrol, PLA filament, and blank and carvacrol-loaded PLA scaffolds. The crystal structures were determined by XRD with Cu Kα radiation (40 kV, 30 mA) on a Philips type powder diffractometer (Amsterdam, Netherlands) fitted with PW1710 control unit, PW1820/00 goniometer and FR590 Enraf Nonius generator, operated at a step size of 0.02° (counting time of 2 s per step) over a 2Θ range of 2–40° at room temperature. DSC analysis was carried out using a DSC Q100 (TA Instruments, New Castle, DE, USA) from 25 to 300°C at a scanning rate of 10°C/min in nitrogen atmosphere (50 mL/min).

2.7. Mechanical properties

Carvacrol-loaded scaffolds were evaluated, in triplicate, using a TA. XT Plus Texture Analyzer (Stable Micro Systems, Surrey, UK) equipped with a 30 kgf (~294 N) load cell. Scaffolds were subjected to 10 successive stress-strain cycles, applying a uniaxial compression along their short axis (height) by downward movement of an aluminum cylinder probe (20 mm in diameter). The activation strength was set at 1 g. In each cycle, scaffolds were compressed until a force of 20 kg (196 N) was reached, and the force-displacement data were recorded for each compression cycle and later converted to engineered stress and strain, using the initial dimensions of the scaffolds (height and diameter). The compressive modulus was calculated as the slope of the initial linear region of the stress-strain curves. Following a similar protocol, the mechanical properties were also evaluated by placing the scaffolds vertically along the diameter and applying the force on the lateral surfaces. The scaffolds were incubated in PBS pH 7.4 at 37°C (protected from light) for 18 months and their appearance and mechanical properties evaluated again.

2.8. Biocompatibility evaluation

Proliferation of human adipose-derived mesenchymal stem cells (adMSCs; PCS-500-011, ATCC, USA) in the presence of scaffolds was evaluated using a colorimetric Cell Counting Kit-8 (CCK-8; Dojindo, Kumamoto, Japan). adMSCs were first expanded in MEM-alpha supplemented with 10% FBS, 1% glutamine (ThermoFisher), and 1% antibiotic-antimycotic solution (penicillin 10,000 IU/mL; streptomycin 10,000 μg/mL; 25 μg/mL Fungizone™). Scaffolds were sterilized by soaking in a 70% ethanol solution for 5 s and then kept in a laminar flow cabinet until ethanol was completely evaporated. Scaffolds were individually placed in wells of a 24-well plate and adMSCs were then seeded at a density of $4{\cdot}10^4$ cells/scaffold and incubated at 37°C, 95% RH and 5% CO_2. At 3, 5, and 7 days of culture, cell proliferation was evaluated following the CCK-8 assay protocol. Briefly, culture medium was withdrawn from wells, and 0.5 mL of CCK-8 working solution were added to each well (10% CCK-8 solution in culture medium) and incubated for 1.5 h at 37°C (95% RH and 5% CO_2). After incubation, the absorbance of individual wells was immediately measured at 450 nm in a microplate reader (UV Bio-Rad Model 680; Hercules, CA, USA). The assay was carried out in quadruplicate. Cell viability was calculated as follows:

$$Cell\ viability\ (\%) = \frac{Abs_{exp} - Abs_{blank}}{Abs_{control} - Abs_{blank}} \times 100 \quad (2)$$

In this equation, exp refers to experimental conditions (cells with scaffolds containing carvacrol), blank refers to CCK-8 working solution (no cells, no scaffolds), and control denotes wells containing cells cultured in culture medium in the presence of control scaffolds (PLA scaffolds).

A Live/Dead viability staining was also used to evaluate the effect of scaffold composition and carvacrol release on cell viability. Scaffolds were sterilized in ethanol as described above and then soaked in FBS for 30 min to favor cell attachment. adMSCs were then seeded on the scaffolds ($4{\cdot}10^4$ cells/scaffold) and cultured in MEM-alpha complete medium at 37°C. After 7 and 12 days of culture, culture medium was removed and scaffolds were washed with PBS. Then, Live-Dead staining was carried out following manufacturer's protocol. Briefly, ethidium homodimer-1 (4 μM) and calcein AM (2 μM) solutions were prepared by dilution of the stock solutions in PBS. Then, culture medium was removed from the wells, and the scaffolds were soaked in PBS and incubated in 1 mL of the working staining solution for 30–45 min at room temperature. Before observation, the solution was removed, and the scaffolds were washed in PBS to reduce background signal and then transferred to microscope slides. Finally, scaffolds were observed using a confocal microscope (Stellaris 8; Leica, Germany).

A hemolytic activity assay was used to determine the blood compatibility of carvacrol and carvacrol-loaded PLA scaffolds and controls by measuring the potential lytic effects of the materials in contact with human erythrocytes. Scaffolds were hydrated in DPBS pH 7.4 for 1 h prior to the assay. Human blood anticoagulated with citrate dextrose solution was provided by the Galician Transfusion Center (ADOS) and obtained from anonymized healthy donors after obtaining written informed consent, in agreement with the Spanish legislation (Law 14/2007 on Biomedical Research). Blood was diluted to a final volume of 3% *v*/v in DPBS pH 7.4 (150 μL blood in 5 mL DPBS). Scaffolds were placed in 15 mL tubes containing 5 mL of the diluted blood and incubated at 37°C for 1 h under oscillatory movement (100 rpm). After incubation, blood samples were centrifuged at 2655*g* for 10 min. Supernatants were transferred in duplicate to 96-well plates, and the absorbance of hemoglobin released in the plasma was measured in a plate reader at 540 nm. Concentrated carvacrol solutions were prepared in ethanol and added to the diluted blood to obtain a final carvacrol concentration of 5, 2.5, 1.25, 0.625, 0.312, 0.156, 0.078 and 0.039 mg/mL (final volume of ethanol 2.5% *v*/v). Triton X-100 1% v/v was used as positive control (hemolytic), while DPBS and ethanol 2.5% v/v were used as negative controls. All conditions were tested in triplicate. The hemolytic activity was calculated as a function of the released hemoglobin by lysed erythrocytes. The percentage of hemolysis (%) was calculated as follows:

$$Hemolysis\ (\%) = \frac{(A_S - A_N)}{(A_P - A_N)} \times 100 \quad (3)$$

where A_S represents sample absorbance; A_N negative control absorbance; and A_P positive control absorbance.

2.9. In ovo tissue integration and angiogenesis evaluation

Integration of scaffolds in the chorioallantoic membrane (CAM) was evaluated using fertilized hen eggs (Coren, San Cibrao das Viñas, Spain). Eggs were placed horizontally in a warm incubator and maintained at 38°C and 60% RH with periodical rotation of the eggs. On day 3, a small window (10 × 10 mm) was opened in the acute pole of the eggs, and a small volume of albumin was aspirated to create an air bag over the CAM to prevent its adhesion to the eggshell that could lead to hemorrhagic events. To prevent the eggs from drying out and contaminate, the windows were covered with transparent film and returned to incubation while maintained in a vertical position. On day 8, scaffolds sterilized as described before were individually placed in direct contact over the CAM (4 replicates per formulation). Eggs were subsequently returned to the incubator until day 12. Then, the CAM was imaged using a 12 MPx digital camera. A score of integration (SI) was given to each scaffold, based on the neovascularization and attachment of the scaffold to the CAM. This score ranged from 0 (poor integration) to 3 (excellent integration) [39].

The integration and vascularization of the scaffolds was further evaluated using micro-CT. Briefly, the CAM surrounding the scaffolds was fixed in 4% paraformaldehyde for 4 h and then, a scaffold-centered circular section of CAM of 30 mm in diameter was collected using a surgical blade. The samples were incubated in Lugol 0.1% for 4 h, then washed 3 times in PBS and scanned using a Skyscan 1272 micro-CT (Bruker; Kontich, Belgium). Scaffolds were scanned before and after implantation using the same scanning conditions. Imaging was carried out at 50 kV and 200 μA, with a 10 μm pixel size, 200 ms exposure time, and 0.2° rotation step. The obtained projections were reconstructed using NRecon software (Bruker) and rendered using CTVox (Bruker). The volume and area of the tissue within the scaffolds were quantitatively evaluated by CTAn software (Bruker) using a volume of interest (VOI) corresponding to the full volume of the scaffolds, using a global thresholding. The evaluation of vessel volume and branches direction in the scaffolds was calculated using CTAn software.

2.10. Anti-biofilm assays

The antimicrobial properties of the carvacrol-loaded scaffolds and PLA controls were evaluated against two bacterial strains commonly related to implant-associated infection, i.e. *Staphylococcus aureus* (ATCC25923, ATCC, Manassas, VA, USA) and *Pseudomonas aeruginosa* (PAO1, Lausanne sub-line, donated by M. Cámara, University of Nottingham) using an active attachment biofilm growth assay and isothermal microcalorimetry.

2.10.1. Modified Amsterdam active attachment (AAA) biofilm cultivation model

The inoculum preparation, bacterial growth and development of the assay were carried out according to a previously described method [40]. *S. aureus* strain was cultured in 1% NaCl Tryptic Soy Broth (TSB-1) and *P. aeruginosa* was cultured in Luria-Bertani's Lysogenic Broth (LB) (10 g/L tryptone; 5 g/L yeast extract, 10 g/L NaCl). Both culture media were prepared in distilled water and autoclaved before use (121°C, 1 atm, 15 min). Scaffolds were sterilized by soaking in 70% ethanol for 5 s and let the ethanol to completely evaporate in a biosafety cabinet at room

temperature. Sterilized scaffolds were then placed in the Amsterdam Active Attachment (AAA) model lid (Figs. S2 and S3, Supplementary Information) making sure that they were fully immersed in the culture media inoculated with the corresponding bacteria (optical density 0.05 for *S. aureus* and 0.01 for *P. aeruginosa*) [41]. The modified AAA biofilm cultivation model makes the entire surface of the scaffolds accessible to bacteria and consequently to active biofilm formation, simultaneously allowing the exchange of the culture medium and the removal of the scaffolds avoiding biofilm damage. All treatments were evaluated in triplicate.

The AAA model was incubated at 37°C in darkness for 48 h for *S. aureus* and 12 h for *P. aeruginosa*. Culture medium was renewed each 12 h by moving the AAA model from the former 24-well plate to a new plate previously filled with 1.5 mL per well. After additional 24 h of incubation with the corresponding bacteria, scaffolds were removed from culture medium and washed three times with phosphate-buffered saline (PBS) pH 7.4 by soaking in 2 mL for 5 min each time. Biofilm formation and bacteria viability on scaffolds were evaluated by determination of colony-forming units (CFUs). After incubation, biofilm was detached in 2 mL of DPBS by sonication for 15 min followed by vortex for 30 s. To determine the number of CFUs, detached-bacteria samples were serial diluted 1:10 by adding 0.5 mL of the bacteria sample to 4.5 mL of TSB-1 or LB medium for *S. aureus* and *P. aeruginosa* respectively. Dilutions $1/10^3$ and $1/10^4$ were seeded in TSA-1 or LB plates by pouring 100 μL of the bacteria dilution and extending it until agar absorbed the liquid and no droplets were observed. Agar plates were incubated at 37°C for 24 h, protected from light. After incubation, bacteria colonies were counted and number of CFUs/scaffold in the original sample calculated taking into account the dilution factor (df) and the total detachment volume (tdv) as follows:

$$\frac{CFUs}{scaffold} = \frac{No.colonies \times df \times tdv\left(\frac{mL}{scaffold}\right)}{volume\ inoculated\ on\ culture\ plate\ (mL)} \quad (4)$$

S. aureus biofilm formation and viability on scaffolds was also evaluated using the Live/Dead® BacLight™ viability assay. Scaffolds with grown biofilms were stained following the kit protocol, and micrographs were acquired using a Confocal Spectral Microscope Leica TCS-SP5 (Leica Microsystems Heidelberg GmbH, Mannheim, Germany).

2.10.2. Isothermal microcalorimetry

Metabolic heat of bacteria was determined in an I-Cal Flex Isothermal calorimeter system (Calmetrix, Needham, MA, USA) equipped with 8 calorimeters (20 mL capacity) and previously stabilized and calibrated at 37°C. Ethanol-sterilized blank and carvacrol-loaded scaffolds were placed in culture medium without (3 mL, controls) or with bacteria (3 mL, tests). Optical densities of *S. aureus* and *P. aeruginosa* were adjusted to 0.1 and 0.01, respectively. Changes in energy as a function of time were recorded as power (mW) for 48 h; data were gathered every 10 s for the first hour and every 1 min for the next 47 h using the I-Cal Logger software. In all runs, two calorimeters were used for the monitoring of culture medium with bacteria without scaffolds. All experiments were carried out two times in duplicate in separate days, and the data were analyzed using I-Cal Reports software and plotted using SigmaPlot v.14.0. After the experiment, scaffolds incubated in culture medium without bacteria were rinsed with water, and the amounts of carvacrol remaining in the scaffolds were quantified after extraction in 5 mL of methanol:ethyl acetate (50:50 *v*/v) mixture as described in Section 2.3.

In other set of experiments, PLA and PLA-CAR 10% scaffolds were placed in a 24-well plate and incubated in 2 mL of *S. aureus* (OD 0.1) or *P. aeruginosa* (OD 0.01) inoculum for 6 h at 37°C. Then, the scaffolds were withdrawn from the bacteria inoculum and washed three consecutive times with sterile culture medium in a 24-well plate to remove planktonic bacteria while keeping the formed biofilm intact on the scaffold surface. Scaffolds with pre-formed biofilm were then placed in calorimeter vials with 3 mL of the corresponding medium (TSB-1 for *S. aureus*; LB for *P. aeruginosa*), introduced in the calorimeter and incubated for 48 h at 37°C, as explained above.

2.11. Statistical analysis

Statgraphics Centurion 18 v. 18.1.13 (Statgraphics Technologies, Inc., Warrenton, VA, USA) software was used to compare formulations using one-way analysis of variance (ANOVA) followed by Multiple Range Test. The level of significance was 0.05.

3. Results and discussion

3.1. Scaffold 3D printing and carvacrol loading

Recently, our group reported that the incorporation of a drug before or after 3D printing may have a profound impact on drug location and release rate from the scaffolds [35]. In the present work, PLA scaffolds were prepared by FFF 3D printing, and carvacrol loading was carried out applying two different strategies: (a) incorporation of carvacrol into a commercial PLA filament which was subsequently used to print the carvacrol-loaded scaffold (coded as F.PLA-CAR), or (b) incorporation of carvacrol in a previously printed PLA scaffold (coded as PLA-CAR) (Table 1). PLA blank scaffolds were also printed and used as carvacrol-free controls. Furthermore, sets of scaffolds with and without (w/o) perimeter were prepared for all compositions. Carvacrol is poorly soluble in water (1.00–1.25 mg/mL) [42], therefore a mixture of methanol and ethyl acetate (50:50 vol/vol) was used as solvent for carvacrol loading. This solvent admixture was used due to the good solubility of carvacrol in methanol, while ethyl acetate reversibly swelled PLA without dissolving it. After a drying step, carvacrol was expected to remain trapped inside the polymer matrix. Carvacrol has a boiling temperature of 237°C [43] and the melting temperature of PLA is 168.5°C [35]. Consequently, the extrusion printing temperature was set to 220°C.

Table 1
Scaffolds prepared with and without (w/o) perimeter, protocol used for carvacrol loading, and final weight, dimensions, and content in carvacrol of each scaffold (mean ± standard deviation).

Scaffold	Loading	Weight (mg)	Height (mm)	Diameter (mm)	Carvacrol content (mg)
PLA	–	138.7 ± 5.40	4.67 ± 0.09	10.49 ± 0.08	–
F.PLA-CAR 10%	Preloaded filament	154.9 ± 8.30	4.67 ± 0.11	10.63 ± 0.07	3.91 ± 0.75
PLA-CAR 5%	Scaffold soaked in carvacrol 5% v/v	145.2 ± 7.70	4.64 ± 0.09	9.76 ± 0.06	4.20 ± 0.37
PLA-CAR 10%	Scaffold soaked in carvacrol 10% *v*/v	147.5 ± 8.1	4.65 ± 0.09	9.80 ± 0.07	6.19 ± 1.00
PLA w/o	–	93.4 ± 4.90	4.51 ± 0.11	9.73 ± 0.08	–
F.PLA-CAR 10% w/o	Preloaded filament	103.1 ± 4.10	4.56 ± 0.10	10.02 ± 0.09	2.65 ± 0.08
PLA-CAR 5% w/o	Scaffold soaked in carvacrol 5% *v*/v	96.8 ± 3.9	4.44 ± 0.12	9.23 ± 0.14	2.59 ± 0.33
PLA-CAR 10% w/o	Scaffold soaked in carvacrol 10% v/v	96.0 ± 6.4	4.46 ± 0.14	9.25 ± 0.17	5.31 ± 0.11

3.2. Structure analysis

Differences in the appearance of the scaffolds were evident when observed at plain sight and under optical microscope (Fig. 1a). Blank PLA scaffolds presented colorless, translucid aspect, with homogeneous and smooth strands. F.PLA-CAR scaffolds (loaded pre-printing) were also colorless and translucid, but the surface of the strands was less smooth, and air bubbles were observed inside the strands. PLA-CAR (loaded post-printing) scaffolds were opaque and whitish, with regular strands. Noticeably, PLA and F.PLA-CAR scaffolds showed smooth strands, while PLA-CAR scaffolds showed significant roughness on the strand surface, as evidenced in more detail in the FESEM micrographs (Fig. 2).

The overall structure of the printed scaffolds was evaluated using micro-CT. Reconstructed samples showed similar dimensions (height, diameter, and pore size) to the 3D model design, demonstrating high design fidelity and reproducibility without substantial differences among scaffold compositions (Table 1, Fig. 1b). Compared to PLA controls, scaffolds loaded with carvacrol after printing (PLA-CAR) experimented a slight reduction in their diameter during the solvent removal step and turned into an opaque whitish color. This finding may be related to conformational changes of the thin PLA strands during exposition to the mixture of organic solvents employed for the loading and subsequent solvent evaporation. Differently, carvacrol-loaded PLA filaments (thicker) did not show any change in their length and diameter. Scaffolds without perimeter (external wall bordering the scaffold) were lighter and showed smaller diameter (Table 1). Regarding scaffold height, no significant differences were observed between scaffolds.

The porous structure of the PLA and PLA-loaded scaffolds was also evaluated by micro-CT (Fig. 1b). Reconstructed samples showed homogeneous pore size and strand width distribution in every condition regardless of the drug loading method and the presence or absence of perimeter in the structure of the scaffolds. The size of the horizontal pores of the carvacrol-loaded PLA scaffolds, in the 525–585 μm range, was not significantly different from the PLA controls. Likewise, the strand width was similar in all the evaluated samples, in the 220–270 μm range. The porosity and pore interconnectivity of the printed scaffolds was also evaluated. All conditions showed a similar porosity of approx. 72% in the central region of the scaffold and the interconnectivity was 100% (throat size threshold of 10 μm). Interconnectivity plays an

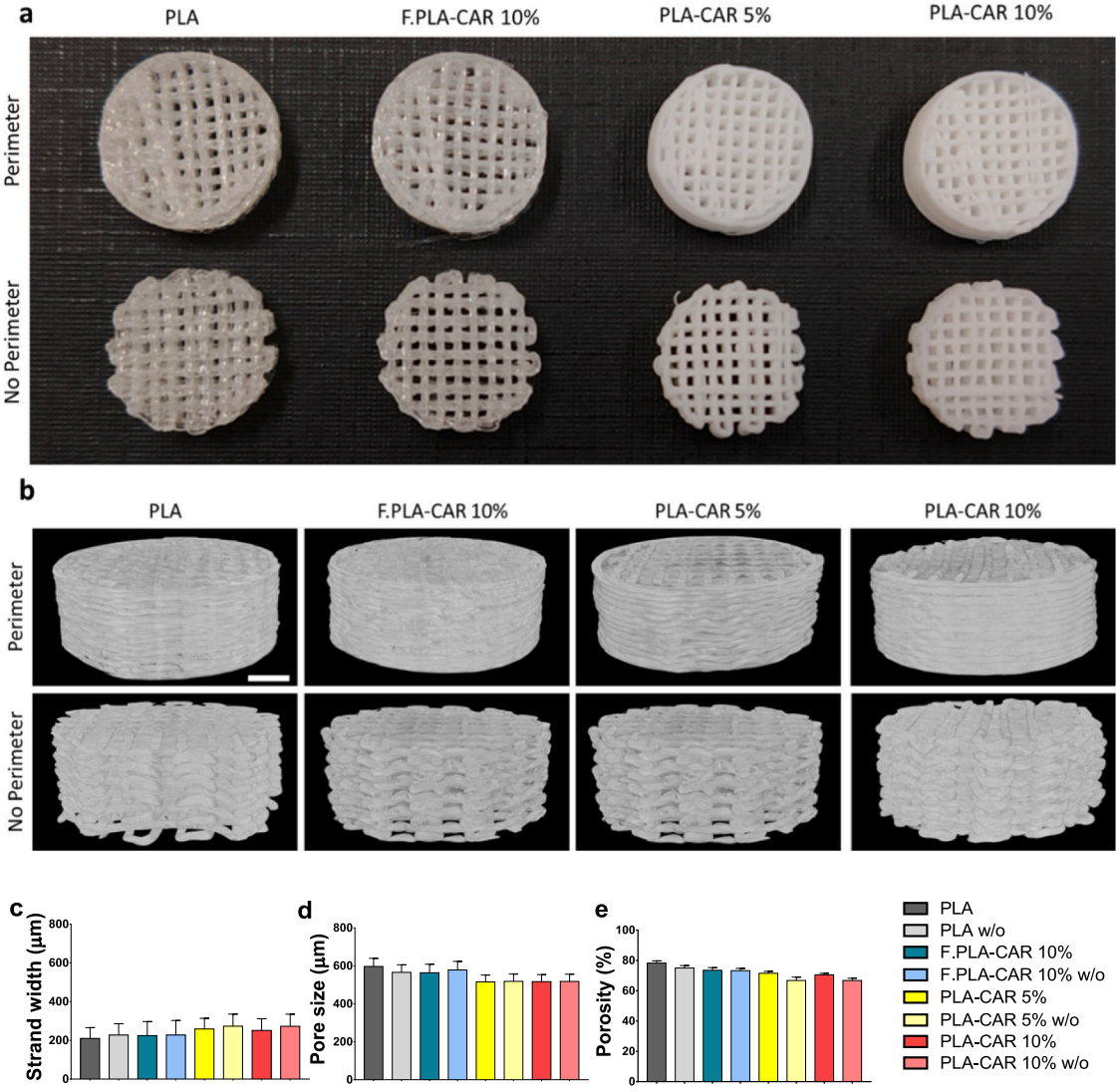

Fig. 1. (a) Appearance of blank PLA scaffolds, carvacrol pre-print loaded (F.PLA-CAR 10%) and post-print loaded (PLA-CAR 5% and 10%) scaffolds. Scaffolds with perimeter (top) and without it (w/o) (down); (b) Representative micro-CT images of the same scaffolds. Scale bar is 2 mm for all reconstructions; (c) Strand width, (d) pore size, and (e) porosity of blank and carvacrol-loaded scaffolds prepared with or without perimeter and evaluated by micro-CT. Each condition is represented as mean ± standard deviation ($n = 5$).

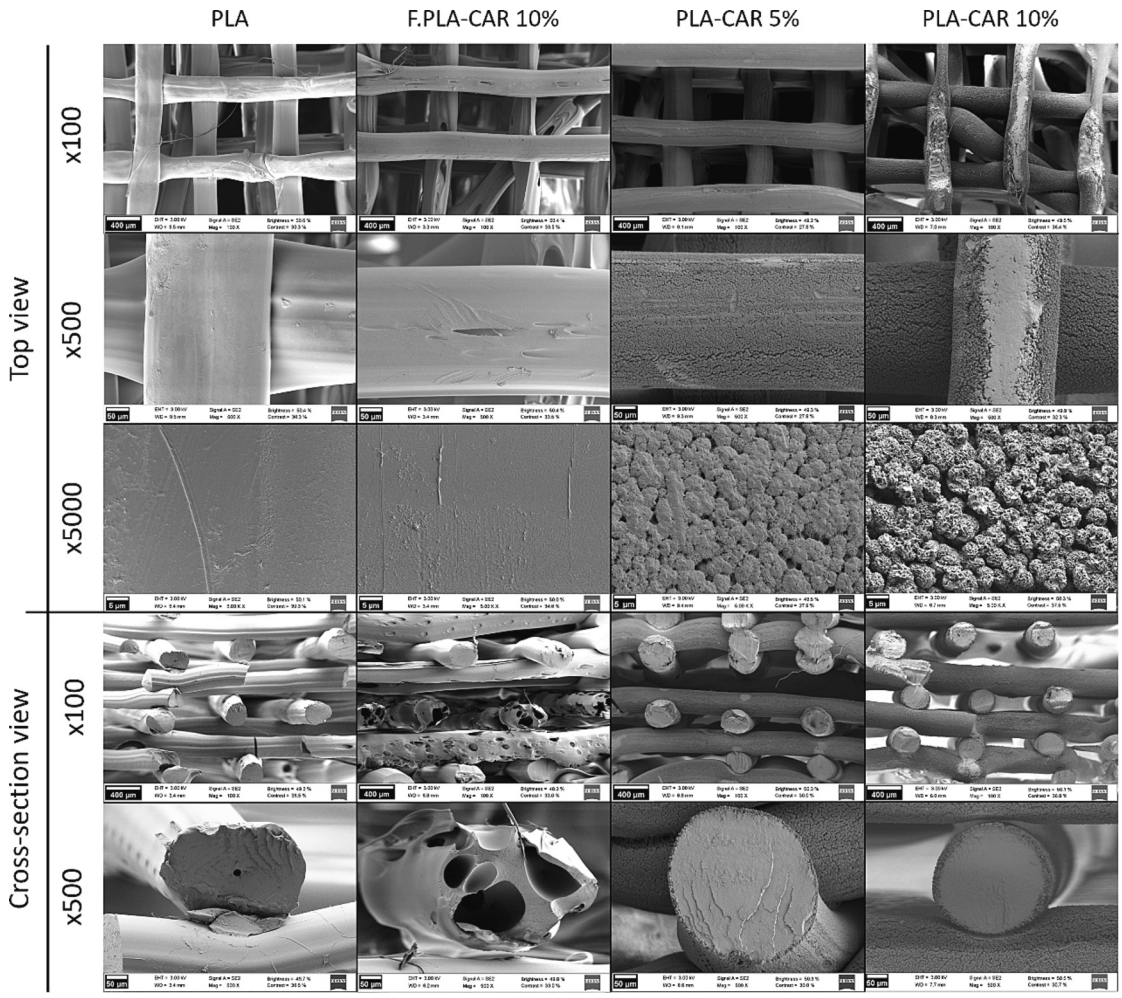

Fig. 2. FESEM images of PLA, PLA pre-printing loaded with carvacrol (F.PLA-CAR 10%) and post-printing loaded (PLA-CAR 5% and 10%) scaffolds.

essential role in tissue engineering by enabling nutrients exchange and cell migration within the structure of the scaffolds [44]. Moreover, an open porous structure significantly facilitates uniform cell migration and scaffold colonization. Although scaffolds with perimeter lack of lateral pores, the upper and lower sides of the scaffolds provided an open, fully interconnected porosity (Figs. S1 and S4, Supplementary Information). The 3D model described here can be adapted to the patient-specific and site requirements of the bone defect by simply changing the filling density and fiber layout.

FESEM imaging allowed for further evaluation of the topography and internal structure of scaffold strands (Fig. 2). The presence of pores in the strands of F.PLA-CAR scaffolds was confirmed. In the FFF 3D printing process, the PLA filaments melted before being extruded into strands. During this melting, carvacrol loaded in the filament was blended with melted PLA at the temperature set for the 3D printing process (220°C). Although carvacrol boiling temperature was not reached, TGA results for carvacrol showed that evaporation starts at temperatures above 90°C (Fig. S5, Supplementary Information). Thus, partial evaporation during the printing process may have caused the pores observed in the strands. PLA-CAR scaffolds (loaded post-printing) showed a rough surface compared to other scaffolds, probably due to the treatment with the solvents used for carvacrol-loading. Indeed, PLA scaffolds soaked in the loading medium without carvacrol also showed a similar modification of the surface.

Regarding surface hydrophilicity, all PLA sheets showed water contact angles below 90°, which is considered a hydrophilic surface. Carvacrol-loaded PLA sheets showed a slight increase in the water contact angles, but it was not statistically significant (Fig. S6, Supplementary Information).

3.3. Carvacrol content

Total carvacrol content in the scaffolds was evaluated by extraction in methanol:ethyl acetate 50:50 *v*/v for 10 days. At day 3, the maximum amount of carvacrol was already extracted, and no significant increase was observed in the following days (Fig. S7, Supplementary Information). As expected, soaking of the scaffolds in loading solutions with higher carvacrol concentrations led to scaffolds containing larger amounts of carvacrol (PLA-CAR 10% 6.61 ± 1.19 mg). Notably, both F.PLA-CAR 10% and PLA-CAR 5% had the same content in carvacrol (3.89 ± 0.52 mg and 3.78 ± 0.34 mg, respectively) despite using different loading methodologies. Scaffolds without perimeter (w/o) loaded less amount of carvacrol compared to their perimeter versions (Table 1), but this can be attributed to their lower mass. Indeed, the amount of carvacrol loaded referred to mass of scaffold was the same for scaffolds with and without perimeter: F.PLA-CAR 10% w/o 25.39 ± 0.54 mg/g; PLA-CAR 5% w/o 27.27 ± 3.54 mg/g; PLA-CAR 10% w/o 55.63 ± 1.83 mg/g.

To the best of our knowledge, there is only one report on 3D printed surfaces that were added with carvacrol for food applications [31]. In that report, the surface of polyethylene terephthalate (PET) printed materials was treated with a solution of carvacrol in water of concentration equals to 0.14 mg/mL and then let to dry. No information was given on the surface area of the printed materials nor on the total volume

of carvacrol used. Moreover, since carvacrol is water insoluble, phase separation was likely to occur. In our case, PLA filament and scaffolds were completely immersed in 5% (i.e., 50 mg/mL) or 10% (i.e., 100 mg/mL) carvacrol solution in methanol:ethyl acetate 50:50 *v*/v mixture, which ensured the complete solubilization of carvacrol and moderate, reversible swelling of PLA in order to promote the diffusion of carvacrol into PLA matrix.

3.4. Carvacrol release

Release profiles were recorded in ethanol:water 1:1 v/v as accelerated release medium, which ensured sink conditions. It has been previously reported that the addition of ethanol to aqueous release media allows obtaining release profiles that simulate those recorded in the *in vivo* nutrient-rich media [45,46]. Results showed that the loading procedure used to incorporate carvacrol notably determined its release profile from scaffolds, in good agreement with a previous report [35]. Carvacrol release rate from F.PLA-CAR scaffolds was slow and sustained over a large period of time (at least 3 months) (Fig. 3 a and b). During the extrusion of carvacrol-loaded filaments, PLA was melted and blended with carvacrol, resulting in strands where carvacrol molecules remained entrapped in the polymer matrix. Therefore, the release of carvacrol may be regulated through PLA hydrolysis-driven mechanism [35,47].

Differently, PLA-CAR 5% and PLA-CAR 10% showed a burst release of carvacrol with 50% and 80% released at 24 h, respectively. Carvacrol was mainly located on the most surface layers of these scaffolds; thus, it could be solved by the release medium quite rapidly. A small portion of carvacrol may had diffused into the polymer matrix, acting as a reservoir of carvacrol that was slowly released during the following days. Carvacrol levels in the release media continued increasing during the first two weeks.

Scaffolds without perimeter (w/o) showed release patterns similar to those recorded for scaffolds with perimeter (Figs. 3 c and d and S8 in Supplementary Information). Scaffolds w/o loaded less carvacrol compared to those with perimeter in absolute values; hence, lower amounts of carvacrol were released. The release of carvacrol from F.PLA-CAR w/o 10% scaffolds was sustained over 90 days, while PLA-CAR w/o 5% and 10% scaffolds showed a burst release of carvacrol during the first 48 h, followed by a sustained release rate in the first weeks after, as occurred with the scaffolds with perimeter. Overall, after 4 months in the release medium F.PLA-CAR 10% scaffolds (with and w/o perimeter) released 3.66 ± 0.30 mg and 2.30 ± 0.36 mg of carvacrol, respectively. PLA-CAR 5% scaffolds (with and w/o perimeter) released 2.94 ± 0.32 mg and 2.40 ± 0.34 mg of carvacrol, respectively. For PLA-CAR 10% scaffolds (with and w/o perimeter), the amounts of carvacrol released were 6.36 ± 0.48 mg and 4.47 ± 0.2 mg, respectively.

Previous studies on carvacrol-loaded materials dealt mostly with electrospun mats. Microfibers (1.5 μm) of blends of PLA and

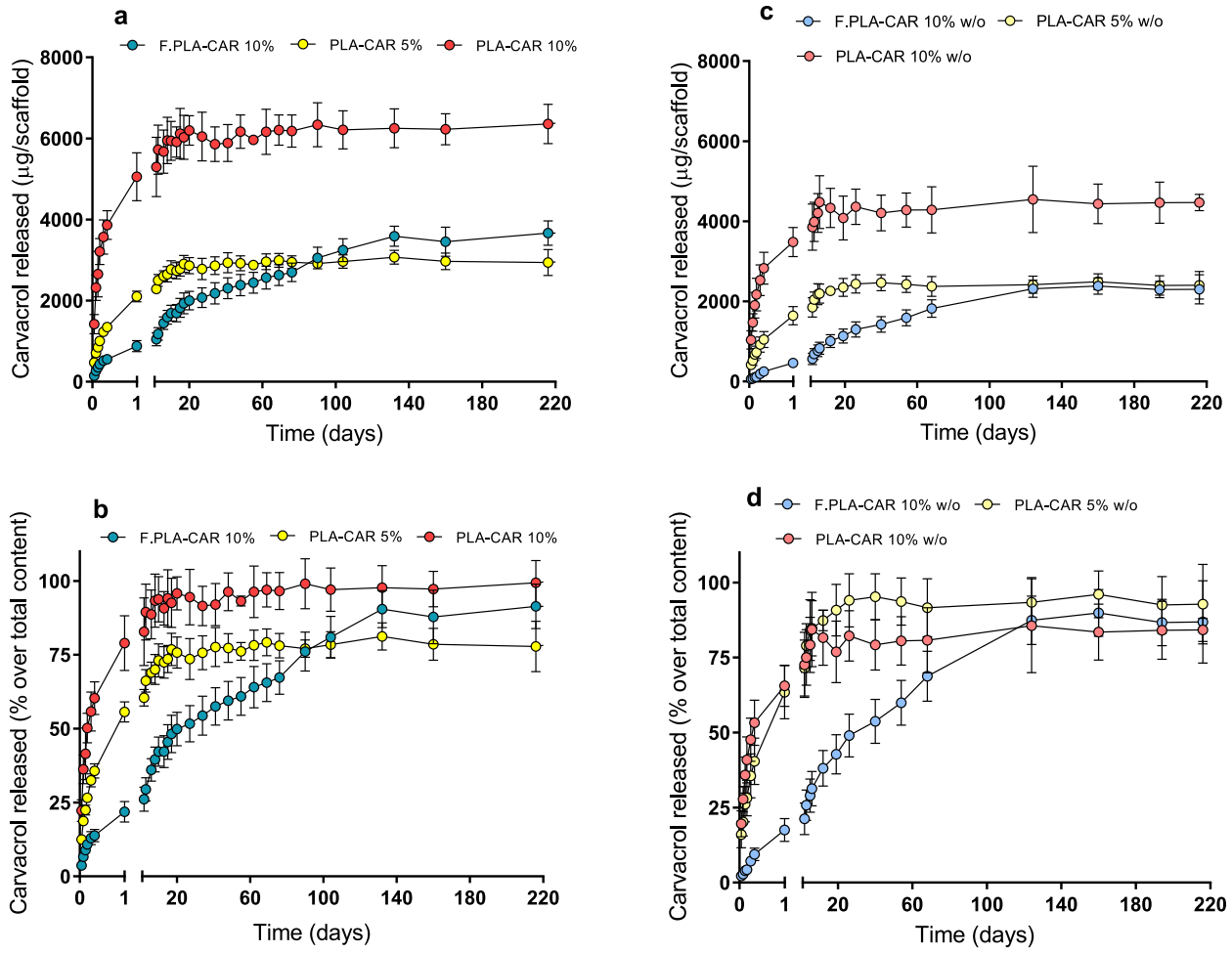

Fig. 3. Carvacrol release profiles from scaffolds: (a,b) scaffolds with perimeter; (c, d) scaffolds without perimeter (w/o). Each scaffold was immersed in 5 mL of ethanol:water (50:50 *v*/v) medium at 37°C and under mild agitation.

polyethylene glycol (PLA/PEG) or polyethylene oxide (PLA/PEO) prepared with carvacrol at 28% with respect to the polymer phase also showed an intense burst in PBS at 37°C, with >60% carvacrol released in 50 h [27]. Microfibers of PLA containing 5 to 20% in carvacrol (1.8–2.2 μm) evaluated after 160 and 350 min at 30°C by headspace gas chromatography–mass spectrometry (GC–MS) also showed relevant burst, which increased with the initial loading in carvacrol [28]. Electrospun mats of poly-(ε-caprolactone) (PCL) containing 12% in carvacrol (200 nm fibers) were evaluated using four different food simulants varying in water contents; namely, the polar media 10% ethanol and 3% acetic acid, the intermediate polar ethanol:water 1:1 *v*/v mixture, and the highly lipophilic isooctane [48]. Carvacrol release rate was markedly faster in the two latter medium, which may be related to both an enhancement in carvacrol solubility (avoiding solubility limitations typical of the more polar media) and a more favorable penetration of the apolar solvent in the polyester matrix, which in turn could facilitate polymer relaxation and swelling [49].

PLA-CAR scaffolds loaded post-printing resembled quite well the fast carvacrol release pattern of the carvacrol-loaded electrospun mats in spite the latter contained carvacrol inside the matrix. Differently, F.PLA-CAR 10% scaffolds (with and w/o perimeter) provided more efficient controlled release even in the ethanol:water 1:1 v/v medium, which may be related both to the lower carvacrol:polymer mass ratio (approx. 2.5%) and the larger diameter of the strands (220–270 μm range) compared to that of the nano/microfibers.

Mathematical analysis of the release plots revealed two regions differing in release rate and mechanism (Fig. S9 in Supplementary Information). Similar patterns have also been reported for other PLA-based devices [27]. According to the coefficients summarized in Table 2, the first region of PLA-CAR scaffolds fitted quite well to Fickian diffusion, which means that carvacrol that had previously been loaded by diffusion towards PLA bulk abandons the scaffold mainly by diffusion through the PLA network. The release rate increased with the content in carvacrol, suggesting that the entry of the release medium and subsequent delivery of carvacrol became facilitated as the PLA proportion decreased. No relevant differences were recorded for scaffolds with and without perimeter. In the second region, most carvacrol was released and the amount remaining in PLA-CAR scaffolds diffused out through pores fill of water, according to the low *n* exponents recorded [50]. F.PLA-CAR 10% scaffolds (with and w/o perimeter) showed higher *n* values in both regions and much lower release rate constant in good agreement with release kinetics recorded for drug-embedded PLA fibers.

Minimum inhibitory concentration (MIC) of carvacrol against *S. aureus* has been reported to be in the 0.20–0.65 mg/mL range depending on the strain [51,52]. In the case of *P. aeruginosa*, carvacrol 0.28 mg/mL has been shown to hinder the production of Quorum Sensing signaling molecules, thus attenuating virulence and cell motility [53]. According to the release profiles, these concentrations could be provided by any of the scaffolds in the first 24 h if immersed in 1 mL medium. The volume could be notably increased in the case of PLA-CAR 10% with and without perimeter (Fig. 3). Moreover, for these latter scaffolds the carvacrol concentration at the surface of the material may higher than the concentration achieved in the surrounding medium because of the hydrophobicity of carvacrol.

Table 2
Fitting of the Korsmeyer-Peppas equation to the mean values of the carvacrol release profile. Coefficients and, in parenthesis, standard errors.

	Region I			Region II		
Scaffold	*n*	K (%·day^{-n})	R^2	*n*	K (%·day^{-n})	R^2
F.PLA-CAR 10%	0.545 (0.053)	25.19 (1.11)	0.954	0.256 (0.006)	22.51 (1.02)	0.990
PLA-CAR 5%	0.469 (0.020)	59.11 (1.04)	0.991	0.072 (0.009)	60.17 (1.02)	0.873
PLA-CAR 10%	0.475 (0.046)	109.40 (1.10)	0.964	0.061 (0.010)	80.35 (1.01)	0.852
F.PLA-CAR 10% w/o	0.694 (0.053)	17.64 (1.11)	0.971	0.311 (0.008)	17.61 (1.02)	0.994
PLA-CAR 5% w/o	0.444 (0.014)	64.31 (1.03)	0.995	0.092 (0.013)	70.19 (1.03)	0.914
PLA-CAR 10% w/o	0.487 (0.022)	94.38 (1.05)	0.992	0.096 (0.019)	67.30 (1.03)	0.859

3.5. Crystalline state

PLA and F.PLA-CAR scaffolds had amorphous structure, without crystalline peaks (Fig. 4 **a**). Differently, PLA-CAR scaffolds (loaded post-printing) showed crystalline peaks at 16.75°, 19.09°, and 22.45° 2θ. To elucidate whether the observed crystalline peaks corresponded to carvacrol or to a polymorphic transition of the polymer, PLA scaffolds and filaments were immersed in the loading medium (methanol:ethyl acetate 50:50 *v*/v) but in the absence of carvacrol. XRD results indicated that soaking in the organic solvents followed by slow evaporation was responsible for the crystallinity peaks observed in PLA filaments and scaffolds. The commercial PLA filament (no treated) showed a small peak at 16.75° 2θ in agreement with its semi-crystalline nature. The high temperature used for printing followed by a fast cooling on the printer platform could have caused amorphization of PLA, thus explaining the absence of peaks for blank PLA scaffolds. In contrast, PLA scaffolds and filaments that were soaked in the organic solvents (treated) showed crystalline peaks that matched those observed for carvacrol-loaded scaffolds, suggesting that PLA treatment with methanol-ethyl acetate mixture induced an increase in PLA crystallinity. In this regard, non-soaked filament and scaffolds remained translucent in appearance (both pre- and post-printing), while treated ones presented an opaque whitish appearance as superficial PLA crystallized, regardless of carvacrol incorporation.

Regarding F.PLA-CAR scaffolds, the loading may cause an increase of the PLA crystallinity in the carvacrol-loaded filaments. However, during the printing process (rapid heating to 220°C and cooling down) the polymer would transition back to an amorphous state, since no crystalline peaks were observed for these scaffolds in the XRD spectra.

DSC results further complemented the data obtained by XRD. PLA and F.PLA-CAR 10% scaffolds showed a cold crystallization peak at approximately 120°C (Fig. 4c), in agreement with previous reports [30]. Differently, cold crystallization was not observed for PLA-CAR 5% and 10% scaffolds (treated). These results, along with the XRD data (Fig. 4 **a and b**), confirmed that the soaking in the organic solvents (methanol: ethyl acetate 1:1 vol/vol) caused the crystallinity increase in PLA-CAR 5% and 10% scaffolds. Indeed, scaffold melting occurred at 170°C, and the increase of PLA crystalline fraction due to the loading treatment conditions was reflected as an increase in the melting enthalpy (ΔH_m) (Table S1, Supporting Information). No significant differences were recorded between PLA-CAR 5% and 10% scaffolds, which means that the content in carvacrol did not cause further changes in the crystallinity.

Despite the reported capability of carvacrol to penetrate through PLA chains [54], carvacrol incorporation did not cause plasticizing effects on the developed scaffolds probably because of its relatively low proportion (2.5–5.5%) compared to PLA. Interaction of the -OH groups of carvacrol and -C=O groups of PLA has been shown to cause changes in glass transition temperature and crystallinity for films prepared with carvacrol proportions of 9% or above [54].

3.6. Mechanical properties and long-term stability

All scaffolds showed an elastic response followed by a plastic (permanent) deformation as the stress increased (Fig. 5). Compressive modulus values were in the 9–12 MPa range in the first compression cycle for all scaffolds; these values are close to those reported for trabecular bone (50–500 MPa) [55] (Fig. 5a). For a given composition and loading treatment, scaffolds without perimeter performed similarly

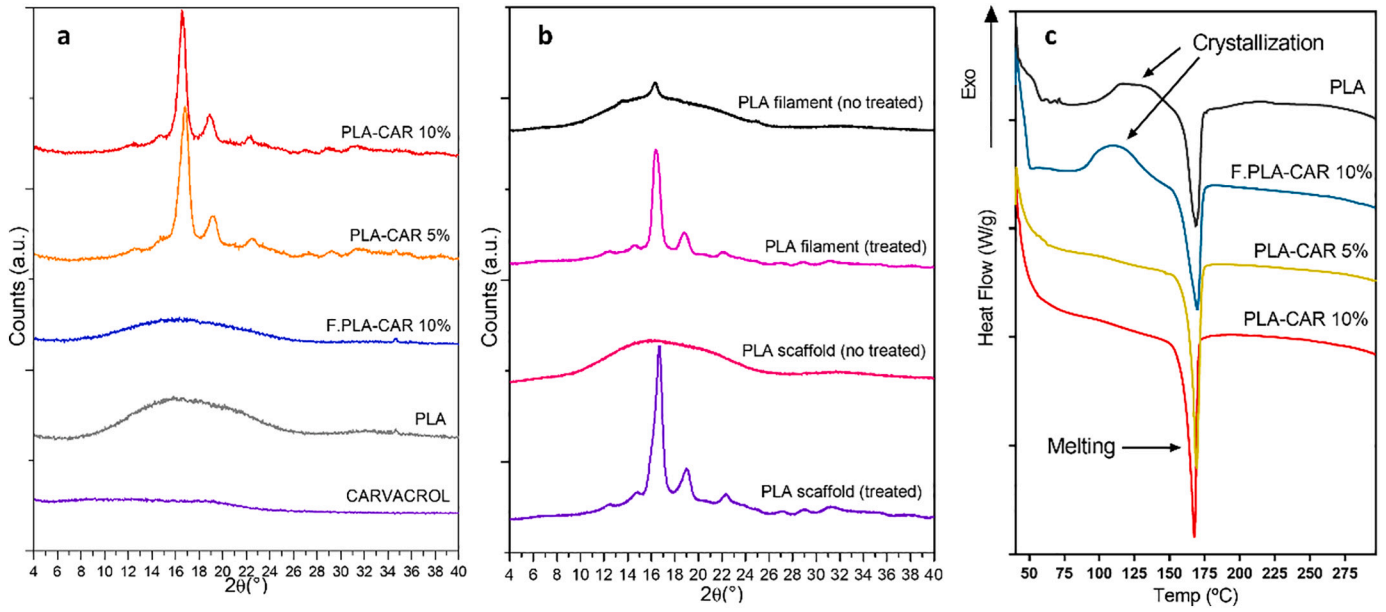

Fig. 4. (a) XRD spectra of carvacrol, PLA, carvacrol-loaded pre-print (F.PLA-CAR 10%) and carvacrol-loaded post-print (PLA-CAR 5% and 10%) scaffolds; (b) XRD spectra of PLA filaments and scaffolds before and after treatment with the loading solvent (methanol:ethyl acetate 1:1, in absence of carvacrol) for 72 h; (c) DSC curves of blank (no treated) and carvacrol-loaded PLA scaffolds.

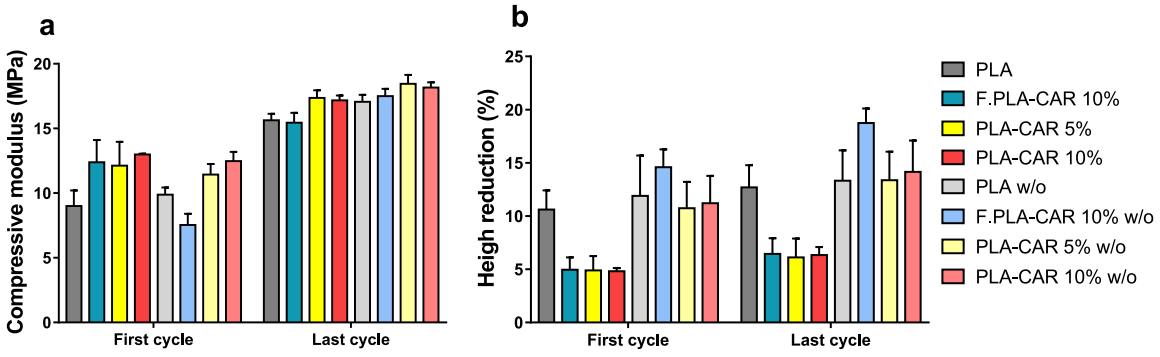

Fig. 5. (a) Compressive modulus values recorded for the 1st and the 10th compression cycle. Scaffolds were subjected to 10 consecutive compression cycles, applying in each one an uniaxial 20 kg-force along the short axis (height) by downward movement (0.5 mm/s) of an aluminum cylinder probe (20 mm in diameter); and (b) permanent deformation of scaffolds during the compression assay estimated from the reduction in scaffold height.

to those with perimeter. However, PLA-CAR 5% and 10% scaffolds loaded post-printing showed higher compressive modulus probably because of the increased crystallinity (as described above). Interestingly, the abundant and deep pores observed in F.PLA-CAR strands did not compromise the mechanical resistance of scaffolds with perimeter but caused a decrease in the compressive modulus and a more intense reduction in height in the F.PLA-CAR scaffold w/o perimeter. These scaffolds showed a remarkable anisotropy when compression was applied laterally, suffering permanent deformation and losing their structural integrity.

PLA solely scaffold with and without perimeter showed a similar reduction in height of approx. 12% after the first compression cycle (Fig. 5b). Interestingly, scaffolds loaded with carvacrol and printed with perimeter were those that deformed less (5.89–6.44%), which might be associated to the concomitant effect of an increase in crystallinity and the lateral reinforcement of the scaffold provided by the perimeter.

We have previously observed that 3D scaffolds prepared with the same PLA filaments incubated in PBS pH 7.4 for 66 days underwent a drop in molecular weight from 150,556 Da (PDI 1.14) to 71,360 Da (PDI 2.04) [35]. Interestingly, no significant changes were recorded in the mechanical properties of the scaffolds. Differently, after 4 months incubation, control PLA scaffolds showed a sharp drop in the mechanical resistance and broke under a force of 196 N. In the present work, all the carvacrol-loaded 3D scaffolds after storage in PBS medium for 18 months showed small changes in the appearance as observed through both optical microscope and SEM images (Figs. S10 and S11, Supplementary Information) but did not withstand the compression cycles and completely collapsed under a 196 N force, disintegrating into small pieces. This suggests that under dynamic in vivo conditions the scaffolds could become soft and completely replaced by the new tissue in few months. Degradation signs were more evident in the surface of blank PLA fibers, compared to carvacrol-loaded fibers, with the presence of abundant cracks throughout the structure of the fibers (Fig. S11). This finding suggested that the hydrophobic carvacrol could protect the fibers from the action of the aqueous environment, but this effect was minor (probably because of the relatively low content in carvacrol) and all scaffolds lost their mechanical properties after prolonged storage in PBS.

3.7. Cyto- and hemo-compatibility studies

PLA is a well-known biocompatible and biodegradable material, but

carvacrol at high concentration may become a skin and eye irritant agent [52]. The viability of adMSCs was evaluated by direct incubation of the cells in the presence of control PLA and carvacrol-loaded scaffolds using a CCK-8 assay (Fig. 6). After 3 days of culture, every condition evaluated led to a cell viability higher than 80%, compared to the PLA control scaffolds. No differences were observed for the scaffolds printed with or without perimeter, as expected. After 5 and 7 days, similar results were observed for all conditions except for F.PLA-10% w/o and PLA-CAR-10% w/o, which showed a significantly decreased cell viability compared to the PLA w/o control probably because of a higher amount of carvacrol released (Fig. 3). Nonetheless, every condition led to cell viability values over 70% after 3 days, compared to the controls, indicating the suitability of the developed scaffolds to preserve the viability of adMSCs, according to the criteria established by ISO 10993-5 for the quantitatively determination of cytotoxicity of implantable materials [56].

The viability of cells developed on the surface of biomaterials is a crucial criterion to evaluate their suitability as implantable scaffolds able to promote and support tissue regeneration. A Live-Dead staining was carried out to evaluate the effect of scaffold composition on adMSCs seeded on the control PLA and carvacrol-loaded scaffolds and cultured for 7 and 12 days (Fig. 7). Cell viability was demonstrated by the presence of a significant monolayer (green-stained cells, alive) grown on the surface of the fibers, in agreement with the viability study. After 7 days, cells seeded on the scaffolds presented elongated cytoplasms, which was indicative of their high viability and spreading ability. Cell density and shape were also maintained after 12 days of culture. Nevertheless, cells seeded on PLA-CAR 10% and PLA-CAR 10% w/o scaffolds showed a significant low density and increased cytotoxicity after 7 days and, more clearly, 12 days of culture. This diminished cell viability can be ascribed to the higher carvacrol concentration on the surface of the scaffold fibers due to the loading strategy (post-printing drug loading).

A hemolysis assay was also carried out to evaluate the effect of the direct contact of the scaffolds with human blood. Diluted blood aliquots that were incubated with carvacrol-loaded scaffolds did not suffer hemolysis, regardless the carvacrol content of scaffolds and the presence or absence of perimeter (Fig. S12, Supplementary Information). Differently, hemolysis was observed when blood was incubated with concentrated carvacrol solutions, and this effect was more intense as carvacrol concentration increased (Figs. S13 and S14, Supplementary Information). The CC_{50} for carvacrol (concentration at which 50% of red blood cells were hemolyzed) was calculated to be around 0.330 mg/mL. While carvacrol solutions were toxic to erythrocytes, carvacrol-loaded scaffolds did not show any toxicity signs probably because of the slow release.

3.8. *In ovo tissue integration and angiogenesis evaluation*

The CAM assay has been recently pointed out as an efficient model with numerous advantages over traditional in vivo studies, including cost effectiveness, availability, and complete accessibility to the circulatory system. Although animal models are still required to test the efficacy and safety of newly developed materials before clinical trials, the lack of reproducible standard animal models for bone regeneration remains a significant drawback of the in vivo studies. Moreover, the accomplishment of reduce, refine, and replace animals in research demands the development of robust alternatives to evaluate the effect of biomaterial implants in the repair of bone and other tissues. The evaluation of the integration and vascularization of scaffolds tested in the CAM is usually approached by histological or macroscopic visual analysis [57]. In the present work, a comprehensive macroscopic and microscopic evaluation was carried out in order to provide a precise tridimensional analysis of the tissue integration and vascularization of the scaffolds. No signs of cytotoxicity or hemolysis were noticed in the tissue surrounding the scaffolds during the incubation period. The macroscopic inspection of the scaffold-CAM region at the end of the incubation time revealed the integration of the scaffolds with the surrounding tissue disregarding the composition. The integration score was very good (3) for scaffolds without perimeter, and large blood vessels were developed around the scaffolds with capillary penetration through open pores (Fig. S15, Supplementary Information). Scaffolds with perimeter were apparently less integrated (scores 0–2) with no lateral vessels.

A thorough evaluation of the degree of integration of the scaffolds with the CAM and their vascularization was carried out using micro-CT. Vascularization of implanted biomaterials is critical to their success and appropriate integration with the surrounding tissue. Micro-CT analysis combined with contrast agents can be used to investigate the vascular architecture and tissue infiltration with high resolution [58,59]. In the present study, scaffolds were stained with 0.1% Lugol for 4 h to obtain uniform penetration of the contrast agent within the specimens with minimal tissue shrinkage. The volume rendering of the reconstructed

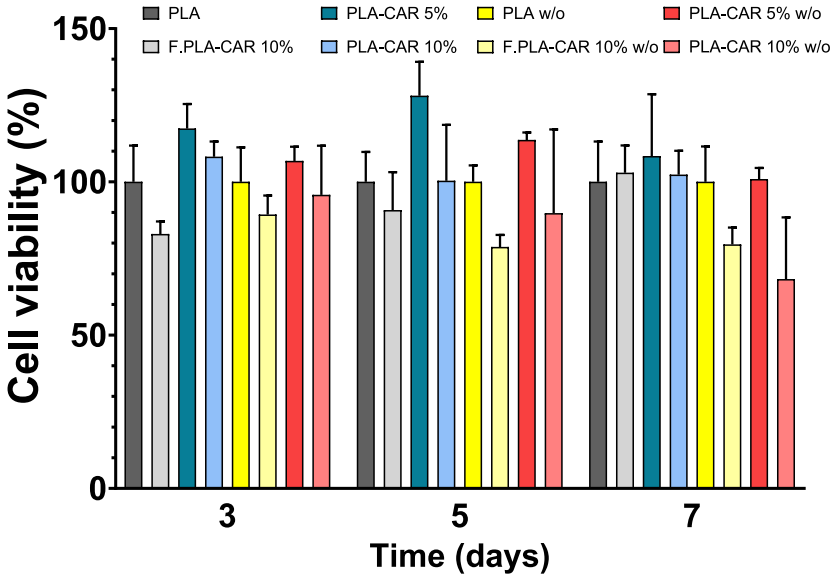

Fig. 6. Viability of adMSCs incubated with control PLA-scaffolds and carvacrol-loaded scaffolds with and without perimeter after 3, 5, and 7 days of culture.

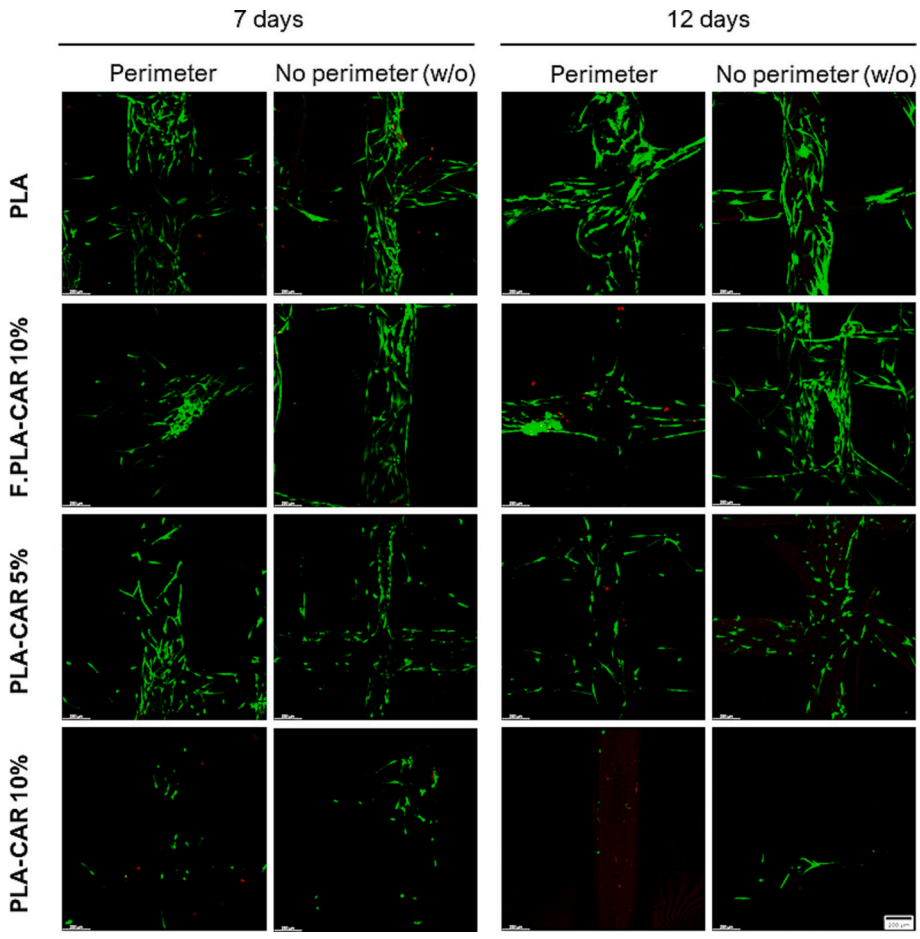

Fig. 7. Merged confocal micrographs of Live/Dead staining, showing cell viability after 7 and 12 days of culture on PLA controls and carvacrol-loaded scaffolds. Live and dead cells are labeled with green and red color, respectively. Scale bar is 200 μm. (For interpretation of the references to color in this figure legend, the reader is referred to the web version of this article.)

projections confirmed the similar extent of tissue integration and vascularization for every composition, as observed in the macroscopic evaluation. Scaffolds with and without perimeter presented large vessels developed in the surroundings of the scaffolds, indicating that the distinct compositions had no detrimental effect on angiogenesis (Fig. 8). Relevantly, scaffolds without perimeter also promoted vasculature development through the open pores in the lateral contour of the scaffolds (Fig. 9). There were no discernible differences ($p > 0.05$) in the total number and volume of the vessels present in the scaffold between the distinct compositions and perimeter structure, suggesting that the incorporation of carvacrol did not lead to any significant decrease in the angiogenic potential of the native tissue. The high number of vessels present in the scaffolds were evident for all compositions, independently of the carvacrol concentration. Such a high vascularization may overcome one of the main barriers to tissue regeneration [60], and indeed the scaffolds' pore size in 525–585 μm is in the range previously identified as optimum to maximize scaffold neovascularization (400–600 μm) [61,62]. Moreover, macropores in this range are known to drive a homogeneous cell distribution throughout the structure of the scaffolds by capillarity mechanism. Compared to previous studies reporting the angiogenic properties of carvacrol through an increase in the release of VEGF by MSCs and triggering of a paracrine angiogenic response [32], no significant differences were found in the promotion of vascularization of scaffolds containing carvacrol, compared to the PLA controls.

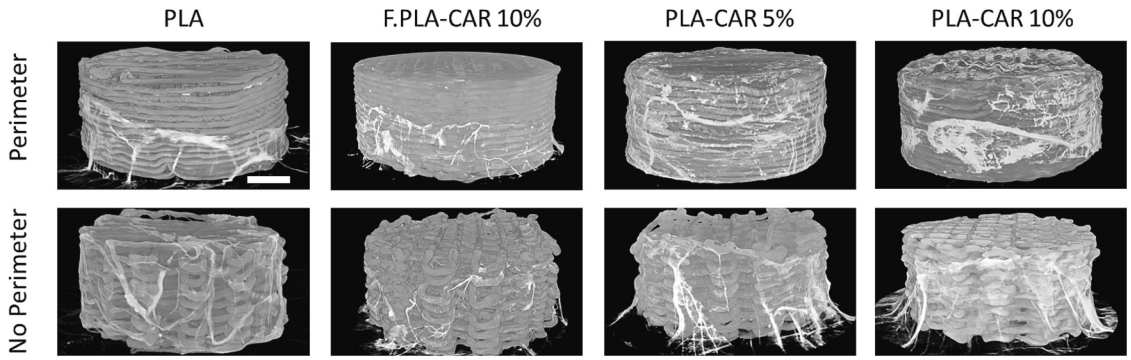

Fig. 8. Representative projections of micro-CT analysis for implanted carvacrol-loaded and control PLA scaffolds. Scale bar: 2 mm.

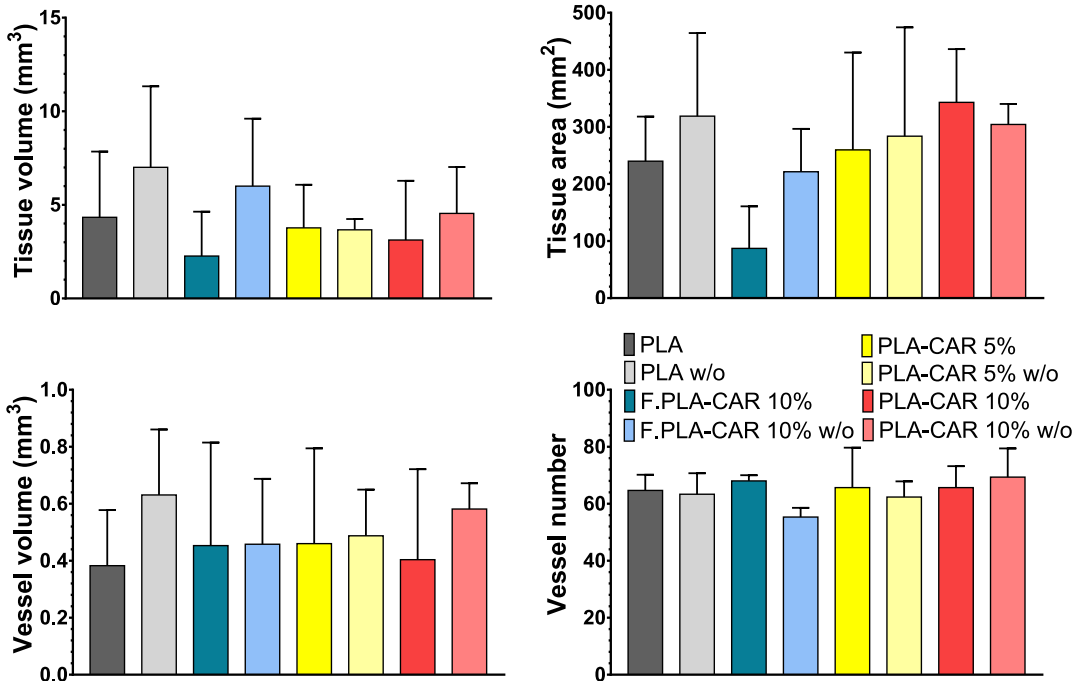

Fig. 9. Tissue volume, tissue area, vessel volume and vessel number, present within the structure of the carvacrol-loaded and control PLA scaffolds, as determined by micro-CT. Data represent mean value ± standard deviation ($n = 4$).

Some recent papers reported that carvacrol may downregulate VEGF expression and could be used in certain oncological treatments [63,64]. In our study, the quantification of the new vessels developed around and inside the scaffolds was similar for all compositions including carvacrol and controls. Therefore, more in depth studies are needed to decipher the role of carvacrol as a pro- or anti-angiogenic drug.

The quantification of tissue infiltration in the scaffolds was also evaluated by micro-CT, using a resolution of 10 μm/pixel. There was no significant enhancement ($p > 0.05$) in the overall tissue development, as demonstrated by the quantification of tissue volume (mm^3) and area (mm^2) present within the structure of the scaffolds. No significant differences were observed between different compositions or perimeter, resulting in tissue volumes in the 3–5 mm^3 range and tissue areas of ca. 100–300 mm^2.

3.9. Anti-biofilm assay

Once the scaffolds demonstrated cytocompatibility and capability to support the development of blood vessels, their suitability to hinder bacteria colonization was explored using two complementary approaches: CFU counting after biofilm formation and metabolic heat monitoring in the presence of the scaffolds. The antimicrobial action of carvacrol is related to its ability to damage bacteria membrane, to decrease intracellular pH and to promote the leakage of potassium and phosphate ions [24,25]. Carvacrol has also demonstrated capability for penetrating through biofilms altering their physical stability [24].

For the first approach, in the AAA model the culture medium (1.5 mL) was renewed each 12 h which limited the amount of carvacrol that could be accumulated in the medium. Despite these challenging conditions, carvacrol-loaded scaffolds showed activity against both *S. aureus*

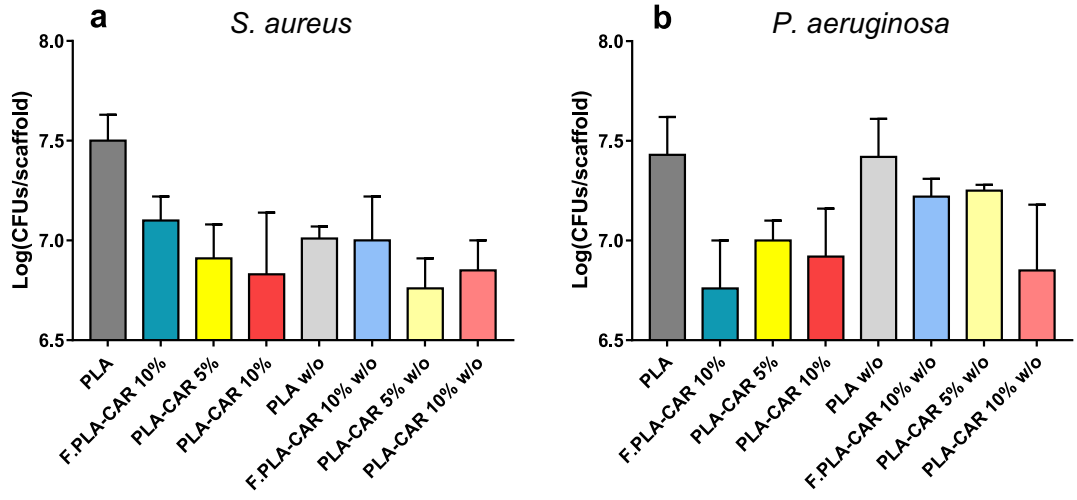

Fig. 10. CFU quantification of (a) *S. aureus* and (b) *P. aeruginosa* biofilms growth on carvacrol-loaded scaffolds after 48 and 12 h of incubation, respectively ($n = 3$).

and *P. aeruginosa* biofilm formation when bacterial colonization was assessed by CFU counting after biofilm detachment (Fig. S16, Supplementary Information). Controls (PLA scaffolds) showed the highest log (CFU/scaffold) of both bacterial species, indicating that biofilm formation was greater in these scaffolds compared to carvacrol-loaded ones (Fig. 10). Carvacrol decreased the CFUs but no statistically significant differences were recorded among the carvacrol-containing scaffolds, probably because carvacrol solubility was limited in the aqueous culture medium where the assay was performed, achieving similar carvacrol concentrations in all cases. Indeed, quantification of resveratrol released in 3 mL culture medium after 48 h incubation was around 10% for all scaffolds. Confocal microscopy of biofilm growth on scaffolds with Live/Dead® staining revealed that *S. aureus* viability on carvacrol-containing scaffolds decreased as carvacrol content increased, compared to PLA scaffolds (Fig. 11; raw images in Fig. S17, Supplementary Information).

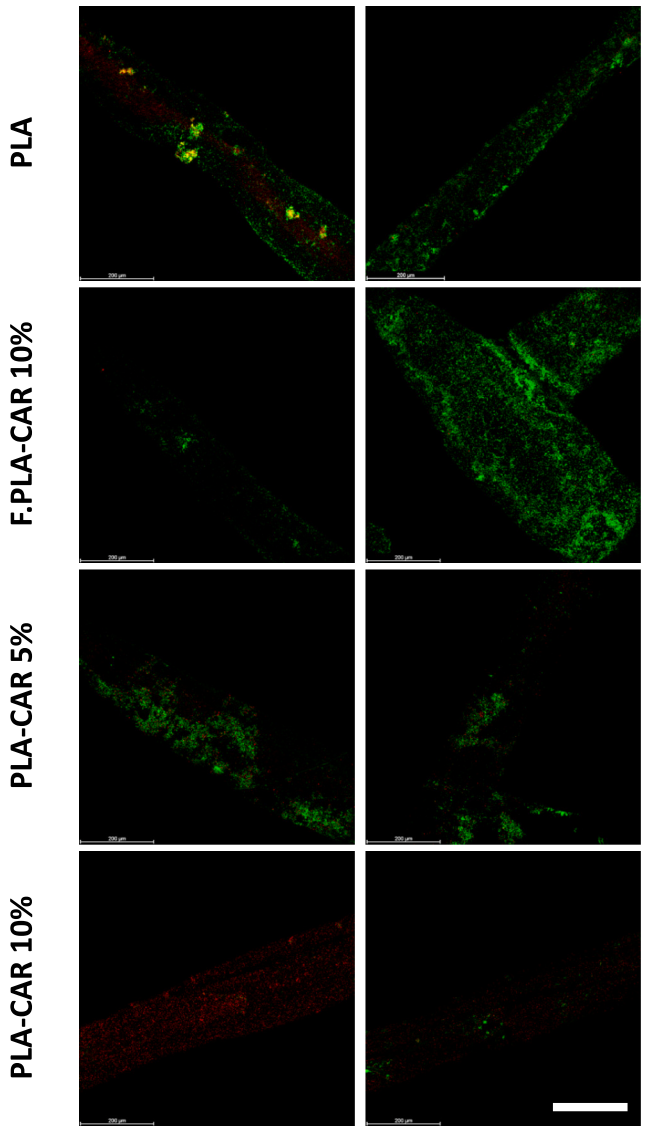

Fig. 11. Confocal microscopy images of Live/Dead® staining of *S. aureus* biofilm growth on carvacrol-loaded scaffolds after 48 h of incubation. Green and red cells correspond to live and dead bacteria, respectively. Two representative regions (right and left) of each scaffold are presented per condition. To avoid the autofluorescence of PLA, the microscope settings were optimized to reduce the background signal without affecting the intensity of red and green stained cells (raw images are available in Fig. S17, Supplementary Information). (For interpretation of the references to color in this figure legend, the reader is referred to the web version of this article.)

Carvacrol in PLA-CAR scaffolds was mainly located at their surface, which could hinder bacterial growth by contact/proximity, even if carvacrol was barely released to culture medium.

Isothermal microcalorimetric analyses were performed to gain further insight into the effects that the scaffolds (carvacrol loading and perimeter) may have on the metabolic activity of the bacteria. Microcalorimetry tests have the advantages of allowing continuous monitoring in real time of the metabolic activity of cells and being highly versatile in terms of volume and turbidity/color since it is label-free and no cell manipulation is necessary [36]. Microcalorimetry also allows to assess the physiological state of the cells within the biofilms [65]. Nevertheless, despite these advantages, calorimetric techniques are still barely applied to evaluate bacteria growth in contact with tissue scaffolds or bone substitutes [37].

First, the scaffolds were monitored for 48 h in the presence of TSB1 and LB media (3 mL) without bacteria to verify that (i) the dissolution and release of carvacrol were not associated to a significant change in energy that may skew the results; and (ii) the scaffolds were indeed sterile, and no growth of other microorganism would occur during the 48 h incubation [66]. All tests carried out in the absence of bacteria led to signals in the −0.02 to +0.02 mW range, which were similar to the signals recorded for the culture media solely (Fig. S18a, Supplementary Information). This means that the treatment applied for scaffolds sterilization ensured the absence of microorganisms and that carvacrol release was not associated to relevant energy exchange. Differently, the incubation of *S. aureus* and *P. aeruginosa* inoculum solely (without scaffolds) caused very remarkable increase in the power recorded (Figs. 12 and S18b, Supplementary Information). The experiments were carried out for 48 h, but the main energy changes occurred in the first few hours.

According to thermokinetic models of bacteria growth previously reported [66], the shape of the heat flow signals revealed an initial high concentration of bacteria with a fast growth rate both in the absence and the presence of the scaffolds. The release of energy was particularly high in the case of *P. aeruginosa* cultures (Fig. 12 **c and d**). Only PLA-CAR 10% scaffolds caused relevant changes in the heat flow signals, inducing a decrease in the energy released in the case of *S. aureus* (Fig. 12 **b**) or a shift of the signal towards greater time values in the case of *P. aeruginosa* (Fig. 12 **d**). These changes clearly indicated that the metabolic activity of the bacteria was significantly altered by the carvacrol released from PLA-CAR 10% scaffolds with perimeter. It should be noted that blank PLA scaffold did not modify the heat flow signals, and also PLA-CAR 10% w/o were not so efficient. This latter finding may be directly related to the higher content in carvacrol of the scaffold prepared with perimeter. In the case of F.PLA-CAR 10% scaffolds no differences were observed between scaffolds with and without perimeter, which may be due to that the release rate of carvacrol from the scaffolds loaded pre-printing was too slow. To gain an insight into the amount of carvacrol released from the scaffolds during the 48 h of static incubation, scaffolds incubated in the culture medium without bacteria were rinsed with water and then extracted in methanol:ethyl acetate (50:50 *v*/v) to determine the amount of carvacrol remanent. The percentage of carvacrol released was 13.23 (s.d. 1.54)% for PLA-CAR 5% and 19.72 (s.d. 9.90)% for PLA-CAR 10%. In the case of F.PLA-CAR 10% scaffolds, the amounts extracted were similar to those loaded, suggesting very minor release to the culture medium. Compared to the carvacrol release profiles recorded in 5 mL of ethanol:water (50:50 v/v) medium (Fig. 3), carvacrol release in bacteria culture medium was slower, which may be related to the limited solubility of carvacrol in a lower volume and more polar medium.

It should be noticed that planktonic growth may be more intense than the growth of bacteria forming biofilm on the scaffold, and thus heat from planktonic bacteria may be overlapping the heat released by sessile bacteria. Thus, to gain an insight into the growth of adhered bacteria, the scaffolds were first incubated for 6 h with the bacterium inoculum and then washed to remove non-adhered bacteria and

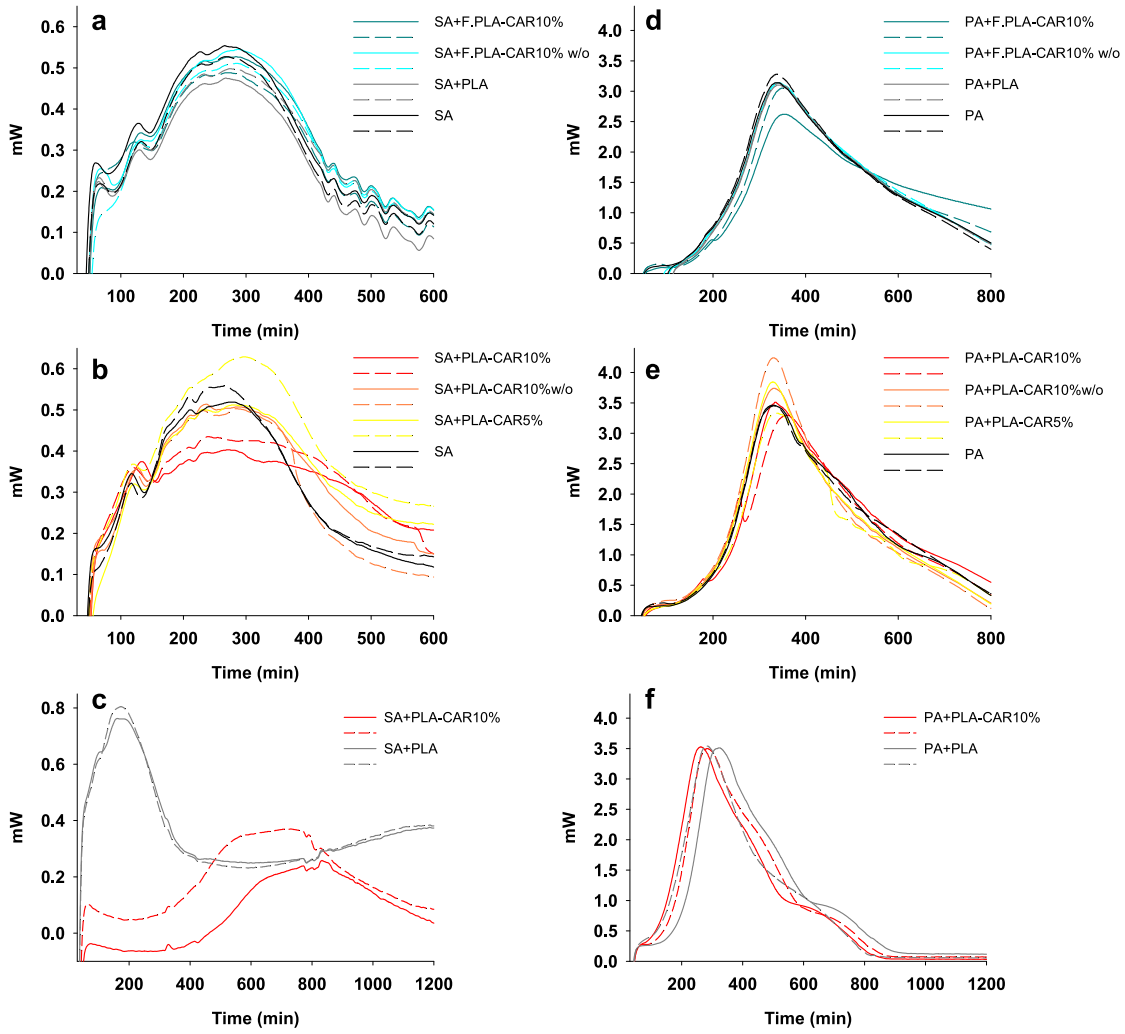

Fig. 12. Isothermal microcalorimetry runs carried out at 37°C for 48 h for scaffolds incubated (a,b,c) with *S. aureus* (OD 0.1) in the TSB1 culture medium, and (d,e,f) with *P. aeruginosa* (OD 0.01). Some scaffolds (a,b,d,e) were incubated with the bacteria inoculum directly (since $t = 0$ min) in the calorimeter vials for 48 h; the first 600 min are depicted in the plots. Another scaffolds (c,f) were first incubated with the bacteria for 6 h in a well-plate, then washed with fresh medium, and then transferred to calorimeter vials containing culture medium and the power monitored for 48 h; the first 1200 min are depicted in the plots. Two replicates are shown for each condition (solid and dotted lines).

incubated again in fresh medium in the calorimeter. After the first 6 h of incubation significant differences ($p < 0.001$) in the turbidity of the inoculum were evident in the wells of *S. aureus*; the OD in the wells containing PLA-CAR10% was of only 0.075 (s.d. 0.017) compared to the values of 1.442 (s.d. 0.071) recorded for wells containing blank PLA scaffolds. Contrary, no significant differences were recorded for the OD of the wells of *P. aeruginosa* incubated with PLA (0.153; s.d. 0.004) or PLA-CAR10% (0.131; s.d. 0.012) ($p = 0.129$). These findings confirmed the higher susceptibility of planktonic *S. aureus* cells to carvacrol released from the scaffolds, compared to *P. aeruginosa.*

In line with these findings, when the scaffolds were washed to remove non-adhered *S. aureus* cells, the microcalorimeter signals recorded for blank PLA scaffolds were remarkably high compared to the attenuated heat flow measured for PLA-CAR10% scaffolds. Indeed, the signal recorded for blank PLA revealed a large number of cells in the exponential phase of growth. Differently, the low initial mW value, long lag time and small peak recorded for PLA-CAR10% scaffolds were typical of low bacteria concentration growing under unfavourable conditions, which confirmed the contact-killing capability of these carvacrol-loaded scaffolds [65,66]. This was not the case for *P. aeruginosa*, and no effects of the carvacrol-releasing scaffolds on cell growth were noticeable.

4. Conclusion

Carvacrol was successfully incorporated in 3D printed PLA scaffolds following two different strategies, which involved either loading the PLA filament pre-printing or loading the scaffold once printed. The loading procedure used notably determined carvacrol location in the strands, and also the crystallinity and mechanical properties of the scaffold. A pre-printing loading resulted in scaffolds where carvacrol was trapped in the polymeric matrix inside the strands, since carvacrol was blended with melted PLA during 3D printing process. Loading post-printing confined carvacrol in the most outer layers of the PLA strands, facilitating fast release, but in parallel caused an increase in PLA crystallinity, which in turn made the scaffolds to became whitish and led to higher compression moduli. Relevantly, carvacrol released from the scaffolds did not have detrimental effects on mesenchymal stem cells compatibility and angiogenesis. Differently, the perimeter (lateral wall) of the scaffold acted as a barrier for lateral vascularization as observed in the CAM model. Scaffolds without perimeter showed better integration in the CAM than perimeter versions as confirmed by micro-CT analysis,

since the open lateral porosity promoted tissue penetration, ingrowth, and angiogenesis, thus aiding scaffold integration and vascularization. The decrease in mass of scaffolds without perimeter, compared to those prepared with the lateral wall, could be responsible for their weaker antimicrobial activity since less carvacrol could be provided to the medium. Only scaffolds prepared with perimeter and loaded post-printing with carvacrol evidenced a significant effect on the metabolic heat of bacteria as recorded using isothermal microcalorimetry. Although all scaffolds loaded post-printing exhibited contact-killing capabilities, further studies may require that the mass of the scaffolds prepared with and without perimeter to be the same since not only carvacrol release rate but also the total amount of carvacrol released play a role in the control of bacteria growth in the surroundings of the scaffold. Although *in vivo* studies are still necessary to evaluate the safety and performance of implantable materials, the introduction of the CAM model and microCT evaluation may serve as a bridge between *in vitro* and *in vivo* evaluation and can help to accomplish the guidelines on reduce, refine, and replace animals in research.

CRediT authorship contribution statement

Xián Farto-Vaamonde: Software, Methodology, Validation, Formal analysis, Data curation, Investigation, Writing – original draft. **Luis Diaz-Gomez:** Methodology, Validation, Formal analysis, Data curation, Writing – original draft. **Ana Parga:** Methodology, Validation, Formal analysis. **Ana Otero:** Methodology, Supervision, Writing – review & editing. **Angel Concheiro:** Conceptualization, Project administration, Resources, Supervision, Funding acquisition, Writing – review & editing. **Carmen Alvarez-Lorenzo:** Methodology, Conceptualization, Project administration, Resources, Supervision, Funding acquisition, Writing – original draft, Writing – review & editing.

Data availability

Data will be made available on request.

Acknowledgments

This work was supported by MCIN/AEI/https://doi.org/10.13039/501100011033 [PID2020-113881RB-I00], FEDER, and Xunta de Galicia [ED431C 2020/17, ED481D-2021-014]. Xián Farto-Vaamonde acknowledges Xunta de Galicia for a predoctoral research fellowship [ED481A-2018/073].

Appendix A. Supplementary data

Supplementary data to this article can be found online at https://doi.org/10.1016/j.jconrel.2022.10.060.

References

[1] Y.C. He, Z. Li, P.G. Alexander, B.D. Ocasio-Nieves, L. Yocum, H. Lin, R.S. Tuan, Pathogenesis of osteoarthritis: risk factors, regulatory pathways in chondrocytes, and experimental models, Biology-Basel 9 (2020) 194.
[2] M. Kloppenburg, F. Berenbaum, Osteoarthritis year in review 2019: epidemiology and therapy, Osteoarthr. Cartil. 28 (2020) 242–248.
[3] J. Hollander, N. Genina, H. Jukarainen, M. Khajeheian, A. Rosling, E. Makila, N. Sandler, Three-dimensional printed PCL-based implantable prototypes of medical devices for controlled drug delivery, J. Pharm. Sci. 105 (2016) 2665–2676.
[4] A.V. Do, B. Khorsand, S.M. Geary, A.K. Salem, 3D printing of scaffolds for tissue regeneration applications, Adv. Healthcare Mater. 4 (2015) 1742–1762.
[5] T. Li, J. Chang, Y.F. Zhu, C.T. Wu, 3D printing of bioinspired biomaterials for tissue regeneration, Adv. Healthcare Mater. 9 (2020) 2000208.
[6] D. Ribatti, T. Annese, R. Tamma, The use of the chick embryo CAM assay in the study of angiogenic activiy of biomaterials, Microvasc. Res. 131 (2020) 104026.
[7] I. Moreno-Jimenez, G. Hulsart-Billstrom, S.A. Lanham, A.A. Janeczek, N. Kontouli, J.M. Kanczler, N.D. Evans, R.O. Oreffo, The chorioallantoic membrane (CAM) assay for the study of human bone regeneration: a refinement animal model for tissue engineering, Sci. Rep. 6 (2016) 32168.
[8] A. Woloszyk, P. Wolint, A.S. Becker, A. Boss, W. Fath, Y. Tian, S.P. Hoerstrup, J. Buschmann, M.Y. Emmert, Novel multimodal MRI and MicroCT imaging approach to quantify angiogenesis and 3D vascular architecture of biomaterials, Sci. Rep. 9 (2019) 19474.
[9] C.T. Johnson, A.J. Garcia, Scaffold-based anti-infection strategies in bone repair, Ann. Biomed. Eng. 43 (2015) 515–528.
[10] W. Zimmerli, P. Sendi, Orthopaedic biofilm infections, APMIS 125 (2017) 353–364.
[11] A. Junka, P. Szymczyk, G. Ziolkowski, E. Karuga-Kuzniewska, D. Smutnicka, I. Bil-Lula, M. Bartoszewicz, S. Mahabady, P.P. Sedghizadeh, Bad to the bone: on in vitro and ex vivo microbial biofilm ability to directly destroy colonized bone surfaces without participation of host immunity or osteoclastogenesis, PLoS One 12 (2017) e0169565.
[12] P.M. Mountziaris, A.G. Mikos, Modulation of the inflammatory response for enhanced bone tissue regeneration, Tissue Eng. B Rev. 14 (2008) 179–186.
[13] M.V. Thomas, D.A. Puleo, Infection, inflammation, and bone regeneration: a paradoxical relationship, J. Dent. Res. 90 (2011) 1052–1061.
[14] J.E. Hellwinkel, Z.M. Working, L. Certain, A.J. Garcia, J.C. Wenke, C.S. Bahney, The intersection of fracture healing and infection: Orthopaedics research society workshop 2021, J. Orthop. Res. 40 (2022) 541–552.
[15] P. Brouqui, M.C. Rousseau, A. Stein, M. Drancourt, D. Raoult, Treatment of Pseudomonas aeruginosa-infected orthopedic prostheses with ceftazidime-ciprofloxacin antibiotic combination, Antimicrob. Agents Chemother. 39 (1995) 2423–2425.
[16] World Health Organization, WHO, Antibacterial Agents in Clinical and Preclinical Development: An Overview and Analysis, Geneva, https://www.who.int/publications/i/item/9789240047655;, 2021.
[17] C.T. Johnson, A.J. Garcia, Scaffold-based anti-infection strategies in bone repair, Ann. Biomed. Eng. 43 (2015) 515–528.
[18] P. Li, Z.W. Gao, Z.W. Tan, J. Xiao, L. Wei, Y.R. Chen, New developments in anti-biofilm intervention towards effective management of orthopedic device related infections (ODRI's), Biofouling 37 (2020) 1–35.
[19] J.S. McLaren, L.J. White, H.C. Cox, W. Ashraf, C.V. Rahman, G.W. Blunn, A. E. Goodship, R.A. Quirk, K.M. Shakesheff, R. Bayston, B.E. Scammell, A biodegradable antibiotic-impregnated scaffold to prevent osteomyelitis in a contaminated in vivo bone defect model, Eur. Cell. Mater. 27 (2014) 332–349.
[20] D.A. Back, N. Bormann, A. Calafi, J. Zech, L.A. Garbe, M. Muller, C. Willy, G. Schmidmaier, B. Wildemann, Testing of antibiotic releasing implant coatings to fight bacteria in combat-associated osteomyelitis - an in-vitro study, Int. Orthop. 40 (2016) 1039–1047.
[21] M.S. Mulani, E.E. Kamble, S.N. Kumkar, M.S. Tawre, K.R. Pardesi, Emerging strategies to combat ESKAPE pathogens in the era of antimicrobial resistance: a review, Front. Microbiol. 10 (2019) 539.
[22] N.B. Sadeer, M.F. Mahomoodally, Antibiotic potentiation of natural products: a promising target to fight pathogenic bacteria, Curr. Drug Targets 22 (2021) 555–572.
[23] R. Iseppi, M. Mariani, C. Condo, C. Sabia, P. Messi, Essential oils: a natural weapon against antibiotic-resistant bacteria responsible for nosocomial infections, Antibiotics (Basel) 10 (2021) 417.
[24] Z.E. Suntres, J. Coccimiglio, M. Alipour, The bioactivity and toxicological actions of carvacrol, Crit. Rev. Food Sci. Nutr. 55 (2015) 304–318.
[25] R.J. Lambert, P.N. Skandamis, P.J. Coote, G.J. Nychas, A study of the minimum inhibitory concentration and mode of action of oregano essential oil, thymol and carvacrol, J. Appl. Microbiol. 91 (2001) 453–462.
[26] M. De Vincenzi, A. Stammati, A. De Vincenzi, M. Silano, Constituents of aromatic plants: carvacrol, Fitoterapia 75 (2004) 801–804.
[27] R. Scaffaro, F.E. Gulino, F. Lopresti, Structure–property relationship and controlled drug release from multiphasic electrospun carvacrol-embedded polylactic acid/polyethylene glycol and polylactic acid/polyethylene oxide nanofiber mats, J. Ind. Text. 49 (2018) 943–966.
[28] A. Altan, Z. Aytac, T. Uyar, Carvacrol loaded electrospun fibrous films from zein and poly(lactic acid) for active food packaging, Food Hydrocoll. 81 (2018) 48–59.
[29] J. Andrade, C. González-Martínez, A. Chiralt, Antimicrobial PLA-PVA multilayer films containing phenolic compounds, Food Chem. 375 (2022) 131861.
[30] I. Armentano, E. Fortunati, N. Burgos, F. Dominici, F. Luzi, S. Fiori, A. Jiménez, K. Yoon, J. Ahn, S. Kang, J.M. Kenny, Bio-based PLA-PHB plasticized blend films: processing and structural characterization, LWT Food Sci. Technol. 64 (2015) 980–988.
[31] S. Er-Rahmani, B. Errabiti, S. Er Raouan, E. Elharchli, A. Elaabedy, S. El Abed, N. El Ghachtouli, M. Sadiki, C. Zanane, H. Latrache, S. Ibnsouda Koraichi, Reduction of biofilm formation on 3D printing materials treated with essential oils major compounds, Ind. Crop. Prod. 182 (2022) 114864.
[32] M.F. Costa, A.O. Durço, T.K. Rabelo, R. de Souza Siqueira Barreto, A.G. Guimaraes, Effects of carvacrol, thymol and essential oils containing such monoterpenes on wound healing: a systematic review, J. Pharm. Pharmacol. 71 (2019) 141–155.
[33] M. Croes, B.C.H. van der Wal, H.C. Vogely, Impact of bacterial infections on osteogenesis: evidence from in vivo studies, J. Orthop. Res. 37 (2019) 2067–2076.
[34] F. Randow, J.D. MacMicking, L.C. James, Cellular self-defense: how cell-autonomous immunity protects against pathogens, Science 340 (2013) 701–706.
[35] X. Farto-Vaamonde, G. Auriemma, R.P. Aquino, A. Concheiro, C. Alvarez-Lorenzo, Post-manufacture loading of filaments and 3D printed PLA scaffolds with prednisolone and dexamethasone for tissue regeneration applications, Eur. J. Pharm. Biopharm. 141 (2019) 100–110.
[36] O. Braissant, A. Bachmann, G. Bonkat, Microcalorimetric assays for measuring cell growth and metabolic activity: methodology and applications, Methods 76 (2015) 27–34.

[37] M. Gonzalez Moreno, M.E. Butini, E.M. Maiolo, L. Sessa, A. Trampuz, Antimicrobial activity of bioactive glass S53P4 against representative microorganisms causing osteomyelitis - real-time assessment by isothermal microcalorimetry, Colloids Surf. B: Biointerfaces 189 (2020), 110853.
[38] J. Siepmann, N.A. Peppas, Higuchi equation: derivation, applications, use and misuse, Int. J. Pharm. 418 (2011) 6–12.
[39] M.L. Ponce, H.K. Kleinmann, The chick chorioallantoic membrane as an in vivo angiogenesis model, Curr. Protoc. Cell Biol. 18 (2003) 19.5.1–19.5.6.
[40] M. Vivero-Lopez, X. Xu, A. Muras, A. Otero, A. Concheiro, S. Gaisford, A.W. Basit, C. Alvarez-Lorenzo, A. Goyanes, Anti-biofilm multi drug-loaded 3D printed hearing aids, Mater. Sci. Eng. C Mater. Biol. Appl. 119 (2021) 111606.
[41] A. Muras, P. Otero-Casal, V. Blanc, A. Otero, Acyl homoserine lactone-mediated quorum sensing in the oral cavity: a paradigm revisited, Sci. Rep. 10 (2020) 9800.
[42] Z.I. Yildiz, A. Celebioglu, M.E. Kilic, E. Durgun, T. Uyar, Fast-dissolving carvacrol/cyclodextrin inclusion complex electrospun fibers with enhanced thermal stability, water solubility, and antioxidant activity, J. Mater. Sci. 53 (2018) 15837–15849.
[43] D.R. Chambre, C. Moisa, A. Lupitu, L. Copolovici, G. Pop, D.M. Copolovici, Chemical composition, antioxidant capacity, and thermal behavior of *Satureja hortensis* essential oil, Sci. Rep. 10 (2020) 21322.
[44] G. Kumar, C.K. Tison, K. Chatterjee, P.S. Pine, J.H. McDaniel, M.L. Salit, M. F. Young, C.G. Simon Jr., The determination of stem cell fate by 3D scaffold structures through the control of cell shape, Biomaterials 32 (2011) 9188–9196.
[45] E. Llorens, L.J. del Valle, J. Puiggalí, Multifunctional ternary drug-loaded electrospun scaffolds, J. Appl. Polym. Sci. 133 (2016) 42751.
[46] R. Zurita, J. Puiggalí, A. Rodríguez-Galan, Triclosan release from coated polyglycolide threads, Macromol. Biosci. 6 (2006) 58–69.
[47] N.F. Zaaba, M. Jaafar, A review on degradation mechanisms of polylactic acid: hydrolytic, photodegradative, microbial, and enzymatic degradation, Polym. Eng. Sci. 60 (2020) 2061–2075.
[48] A. Tampau, C. Gonzalez-Martínez, A. Chiralt, Release kinetics and antimicrobial properties of carvacrol encapsulated in electrospun poly-(ε-caprolactone) nanofibres. Application in starch multilayer films, Food Hydrocoll. 79 (2018) 158–169.
[49] R. Requena, M. Vargas, A. Chiralt, Release kinetics of carvacrol and eugenol from poly(hydroxybutyrate-co-hydroxyvalerate) (PHBV) films for food packaging applications, Eur. Polym. J. 92 (2017) 185–193.
[50] M.I. Rial-Hermida, N.M. Oliveira, A. Concheiro, C. Alvarez-Lorenzo, J.F. Mano, Bioinspired superamphiphobic surfaces as a tool for polymer- and solvent-independent preparation of drug-loaded spherical particles, Acta Biomater. 10 (2014) 4314–4322.
[51] M. Tenci, S. Rossi, C. Aguzzi, E. Carazo, G. Sandri, M.C. Bonferoni, P. Grisoli, C. Viseras, C.M. Caramella, F. Ferrari, Carvacrol/clay hybrids loaded into in situ gelling films, Int. J. Pharm. 531 (2014) 676–688.
[52] S. García-Salinas, H. Elizondo-Castillo, M. Arruebo, G. Mendoza, S. Irusta, Evaluation of the antimicrobial activity and cytotoxicity of different components of natural origin present in essential oils, Molecules 23 (2018) 1399.
[53] M.R. Tapia-Rodriguez, A.T. Bernal-Mercado, M.M. Gutierrez-Pacheco, F. J. Vazquez-Armenta, A. Hernandez-Mendoza, G.A. Gonzalez-Aguilar, M. A. Martinez-Tellez, F. Nazzaro, J.F. Ayala-Zavala, Virulence of *Pseudomonas aeruginosa* exposed to carvacrol: alterations of the quorum sensing at enzymatic and gene levels, J. Cell. Commun. Signal. 13 (2019) 531–537.
[54] D. Briassoulis, I.G. Athanasoulia, P. Tserotas, PHB/PLA plasticized by olive oil and carvacrol solvent-cast films with optimised ductility and physical ageing stability, Polym. Degrad. Stab. 200 (2022) 109958.
[55] E.B.W. Giesen, T.M.G.J. Van Eijden, The three-dimensional cancellous bone architecture of the human mandibular condyle, J. Dent. Res. 79 (2000) 957–963.
[56] International Organization for Standardisation, ISO 10993-5:2009 Biological Evaluation of Medical Devices—Part 5: Tests for In Vitro Cytotoxicity, 2009.
[57] L. Dew, S. MacNeil, C.K. Chong, Vascularization strategies for tissue engineers, Regen. Med. 10 (2015) 211–224.
[58] J.D. Boerckel, D.E. Mason, A.M. McDermott, E. Alsberg, Microcomputed tomography: approaches and applications in bioengineering, Stem Cell Res Ther 5 (2014) 144.
[59] L. Zagorchev, P. Oses, Z.W. Zhuang, K. Moodie, M.J. Mulligan-Kehoe, M. Simons, T. Couffinhal, Micro computed tomography for vascular exploration, J. Angiogenes. Res. 2 (2010) 7.
[60] M. Lovett, K. Lee, A. Edwards, D.L. Kaplan, Vascularization strategies for tissue engineering, Tissue Eng. B Rev. 15 (2009) 353–370.
[61] X. Wang, Z. Nie, J. Chang, M.L. Lu, Y. Kang, Multiple channels with interconnected pores in a bioceramic scaffold promote bone tissue formation, Sci. Rep. 11 (2021) 20447.
[62] H. Mehdizadeh, S. Sumo, E.S. Bayrak, E.M. Brey, A. Cinar, Three-dimensional modeling of angiogenesis in porous biomaterial scaffolds, Biomaterials 34 (2013) 2875–2887.
[63] K. Fatima, S. Luqman, A. Meena, Carvacrol arrests the proliferation of hypopharyngeal carcinoma cells by suppressing ornithine decarboxylase and hyaluronidase activities, Front. Nutr. 9 (2022) 857256.
[64] I. Khan, M. Bhardwaj, S. Shukla, H. Lee, M.H. Oh, V.K. Bajpai, Y.S. Huh, S.C. Kang, Carvacrol encapsulated nanocarrier/nanoemulsion abrogates angiogenesis by downregulating COX-2, VEGF and CD31 in vitro and in vivo in a lung adenocarcinoma model, Colloids Surf. B: Biointerfaces 181 (2019) 612–622.
[65] M.E. Butini, G. Abbandonato, C. Di Rienzo, A. Trampuz, M. Di Luca, Isothermal microcalorimetry detects the presence of persister cells in a *Staphylococcus aureus* biofilm after vancomycin treatment, Front. Microbiol. 10 (2019) 332.
[66] C. Fricke, H. Harms, T. Maskow, Rapid calorimetric detection of bacterial contamination: influence of the cultivation technique, Front. Microbiol. 10 (2019) 2530.